Design and Evaluation of the First Special Sensor Microwave Imager/Sounder

David B. Kunkee, *Senior Member, IEEE*, Gene A. Poe, *Member, IEEE*, Donald J. Boucher, Steven D. Swadley, *Member, IEEE*, Ye Hong, John E. Wessel, and Enzo A. Uliana

***Abstract*—The first Special Sensor Microwave Imager/Sounder (SSMIS) was launched in October 2003 aboard the Air Force Defense Meteorological Satellite Program (DMSP) F-16 Spacecraft. As originally conceived, the SSMIS integrates the imaging capabilities of the heritage DMSP conically scanning Special Sensor Microwave/Imager sensor with the cross-track microwave sounders Special Sensor Microwave Temperature and Special Sensor Microwave Humidity Sounder, SSM/T-2 into a single conically scanning 24-channel instrument with extended sounding capability to profile the mesosphere. As such, the SSMIS represents the most complex operational satellite passive microwave imager/sounding sensor flown while, at the same time, offering new and challenging capabilities associated with radiometer channels having common fields of view, uniform polarizations, and fixed spatial resolutions across the active scene scan sector. A comprehensive end-to-end calibration/validation (cal/val) of the first SSMIS initiated shortly after launch was conducted under joint sponsorship by the DMSP and the Navy Space and Warfare Systems Command. Herein, we provide an overview of the SSMIS instrument design, performance characteristics, and major cal/val results. Overall, the first SSMIS instrument exhibits remarkably stable radiometer sensitivities, meeting requirements with considerable margin while providing high-quality imagery for all channels. Two unanticipated radiometer calibration anomalies uncovered during the cal/val—sun intrusion into the warm-load calibration target and antenna reflector emissions—required significant attention during the cal/val program. In particular, the tasks of diagnosing the root cause(s) of these anomalies as well as the development of ground processing software algorithms to mitigate their impact on F-16 SSMIS and hardware fixes on future instruments necessitated the construction of extensive analysis and simulation tools. The lessons learned from the SSMIS cal/val and the associated analysis tools are expected to play an important role in the design and performance evaluation of future passive microwave imaging and sounding instruments as well as guiding the planning and development of future cal/val programs.**

***Index Terms*—Calibration, meteorology, microwave radiometry, weather forecasting.**

List of Acronyms

AFWA	Air Force Weather Agency.
APMIR	Airborne Polarimetric Microwave Imaging Radiometer.
AMSU	Advanced Microwave Sounding Unit.
CoSMIR	Conical Scanning Microwave Imaging Radiometer.
DMSP	Defense Meteorological Satellite Program.
ECMWF	European Centre for Medium-range Weather Forecasts.
ECTBP	Empirically Corrected Brightness Temperature Processor.
EDR	Environmental Data Record.
EDRP	Environmental Data Record Processor.
EIA	Earth Incidence Angle.
ETL	Environmental Technology Laboratory.
FNMOC	Fleet Numerical Meteorology and Oceanographic Center.
FOV	Field of View.
GDPS	Ground Data Processing Software.
JTWC	Joint Typhoon Warning Center.
LAS	Lower Atmospheric Sounding.
LIDAR	Light Detection and Ranging.
LCP	Left-hand Circular Polarization.
NCEP	National Center for Environmental Prediction.
NEDT	Noise-Equivalent Difference Temperature.
NHC	National Hurricane Center.
NIC	National Ice Center.
NGES	Northrop-Grumman Electronic Systems.
NPOESS	National Polar-orbiting Operational Environmental Satellite System.
NRL	Naval Research Laboratory.
NWP	Numerical Weather Prediction.
MLI	Multilayer Insulation.
RAOB	Radiosonde Observation.
RCP	Right-hand Circular Polarization.
RTM	Radiative Transfer Model.
SAW	Surface Acoustic Wave.
SDR	Sensor Data Record (brightness temperature).
SDRP	Sensor Data Record Processor.
SPAWAR	Space and Naval Warfare Systems.
SSM/I	Special Sensor Microwave Imager.
SSMIS	Special Sensor Microwave Imager/Sounder.
SSM/T	Special Sensor Microwave Temperature.
TDRP	Temperature Data Record Processor.
UAS	Upper Atmospheric Sounding.

Manuscript received March 15, 2007; revised June 23, 2007.

D. B. Kunkee, D. J. Boucher, Y. Hong, and J. E. Wessel are with The Aerospace Corporation, Los Angeles, CA 90009-2957 USA (e-mail: David.Kunkee@aero.org).

G. A. Poe is with the Naval Research Laboratory, Monterey, CA 93943-5502 USA.

S. D. Swadley is with METOC Consulting, Monterey, CA 93943-5598 USA.

E. A. Uliana is with the Interferometrics, Inc., Herndon, VA 20171 USA.

Color versions of one or more of the figures in this paper are available online at http://ieeexplore.ieee.org.

Digital Object Identifier 10.1109/TGRS.2008.917980

I. Introduction

THE FIRST Special Sensor Microwave Imager/Sounder (SSMIS, Serial Number 2) was launched on October 18, 2003 1723Z from Vandenberg Air Force Base, CA, aboard

Fig. 1. Deployed SSMIS instrument showing the main canister, reflector antenna, and calibration load assembly.

the Defense Meteorological Satellite Program (DMSP) F-16 Spacecraft by the last Titan II vehicle. Built by the Northrop-Grumman Electronic Systems (NGES) Company under the direction of the Air Force DMSP Office, the SSMIS represents a joint Air Force/Navy operational program to obtain synoptic maps of critical atmospheric, oceanographic, and land parameters to support Numerical Weather Prediction (NWP) as well as military and civilian users. The first of five instruments scheduled for launch over the next decade, the SSMIS (Fig. 1) is a 24-channel high-precision multifrequency microwave radiometer (Table I) that replaces the current DMSP microwave sounders Special Sensor Microwave Temperature (SSM/T), Special Sensor Microwave Humidity Sounder (SSM/T-2), and Special Sensor Microwave/Imager (SSM/I) while also extending the temperature sounding to the mesosphere (10–0.03 mb). Employing the SSM/I type conical scan geometry, the SSMIS maintains uniform spatial resolution, polarization purity, and common concentric fields of view (FOV) for all channels across the swath (1700 km; Fig. 2). The DMSP F-16 spacecraft flies in a circular sun-synchronous near-polar orbit at an altitude of approximately 833 km with an inclination of 98.9°, orbit period of 101.8 min, and a local time ascending node of 19:54.

The passbands and polarizations selected for SSMIS are based largely on the heritage sensors SSM/T, SSM/T-2, and SSM/I in conjunction with sensor requirements derived from Environmental Data Record (EDR) performance analyses conducted during the sensor design phase by the instrument manufacturer. The center frequencies, bandwidths, and frequency stabilities of the lower air temperature sounding channels, 1–7, are similar to those employed by SSM/T, whereas the humidity sounding frequencies, passbands, and stabilities, of Channels 8–11, are nearly the same as SSM/T-2. The horizontal polarization was selected for the sounding channels that sense the surface emissions based on EDR performance analyses. Based on the success of the SSM/I instrument [1], the SSM/I frequencies and polarizations were selected, with the exception of changing 85.5 to 91.655 GHz to reduce hardware complexity, along with the SSM/I conical scan geometry and external calibration approach. The upper air channel frequencies and passbands are based on internal EDR performance studies by NGES. It should be noted that the receiver polarization for the upper air channels is left-hand circular (LCP) using the IEEE definition of circular polarization as noted in Table I; however, the main reflector reverses the polarization to right-hand circular (RCP) so that the instrument is really sensing RCP of the upwelling partially polarized energy. The weighting functions for the lower air temperature sounding channels are presented in Fig. 3 for a standard atmosphere along with nominal polar and equatorial weighting functions for the upper air channels [2].

Spacecraft interface requirements dictated limits of instrument FOV, size, power, and weight, which in turn restricted the antenna aperture size, number of channels, data rate, and swath. The antenna reflector design is the same as SSM/I but, to accommodate the wide range of frequencies, a multiple-horn frequency multiplexing approach was selected to obtain the desired spatial resolutions (horizontal cell sizes) and high main beam efficiencies with low feedhorn spillover loss and cross-polarization coupling. In addition, the task of integrating a large number of highly sensitive receiver electronics within one instrument presented a number of unique and very challenging "packaging," state-of-the-art component development, and electromagnetic compatibility issues to achieve the requisite calibration accuracies and radiometer sensitivities. Consequently, the SSMIS development process was not an easy one as many components and subsystems resisted passing rigorous tests, resulting in a protracted development cycle. Many lessons learned were captured along the way and are being applied to future design activities, specifically the microwave imager for the National Polar-orbiting Operational Environmental Satellite System.

II. Sensor Design

The SSMIS instrument consists of six major subsystems: antenna/calibration, receiver, signal processing, scan drive, deployment, and structural/thermal (Fig. 4). The antenna/calibration subsystem, in turn, consists of the main reflector,

TABLE I
SSMIS SENSOR CHARACTERISTICS (S/N 02) ON DMSP F-16

Channel	Center Freq.(GHz)	3-db Width (MHz)	Freq. Stab.(MHz)	Pol.	NEDT (K)	Sampling Interval(km)
1	50.3	380	10	*V	0.34	37.5
2	52.8	389	10	*V	0.32	37.5
3	53.596	380	10	*V	0.33	37.5
4	54.4	383	10	*V	0.33	37.5
5	55.5	391	10	*V	0.34	37.5
6	57.29	330	10	RCP	0.41	37.5
7	59.4	239	10	RCP	0.40	37.5
8	150	1642(2)	200	H	0.89	12.5
9	183.31+/-6.6	1526(2)	200	H	0.97	12.5
10	183.31+/-3	1019(2)	200	H	0.67	12.5
11	183.31+/-1	513(2)	200	H	0.81	12.5
12	19.35	355	75	H	0.33	25
13	19.35	357	75	V	0.31	25
14	22.235	401	75	V	0.43	25
15	37	1615	75	H	0.25	25
16	37	1545	75	V	0.20	25
17	91.655	1418(2)	100	V	0.33	12.5
18	91.655	1411(2)	100	H	0.32	12.5
19	63.283248 +/-0.285271	1.35(2)	0.08	RCP	2.7	75
20	60.792668 +/-0.357892	1.35(2)	0.08	RCP	2.7	75
21	60.792668 +/-0.357892 +/-0.002	1.3(4)	0.08	RCP	1.9	75
22	60.792668 +/-0.357892 +/-0.0055	2.6(4)	0.12	RCP	1.3	75
23	60.792668 +/-0.357892 +/-0.016	7.35(4)	0.34	RCP	0.8	75
24	60.792668 +/-0.357892 +/-0.050	26.5(4)	0.84	RCP	0.9	37.5

Notes:
1. Sampling refers to along scan direction based on 833km spacecraft altitude.
2. NEDT for instrument temperature 0 C and calibration target 260K with integration times of 8.4 msec for Chs. 12-16; 12.6 msec for Chs.1-11, 17-18, 24; and 25.2 msec for Chs. 19-23.
3. Number of sub-bands is indicated by (n) next to individual 3-db width. RCP denotes right-hand circular polarization.

* Channels 1 – 5 (LAS) were incorrectly designed as V-pol on unit S/N 02. All other SSMIS Flight units will be configured as H-pol.

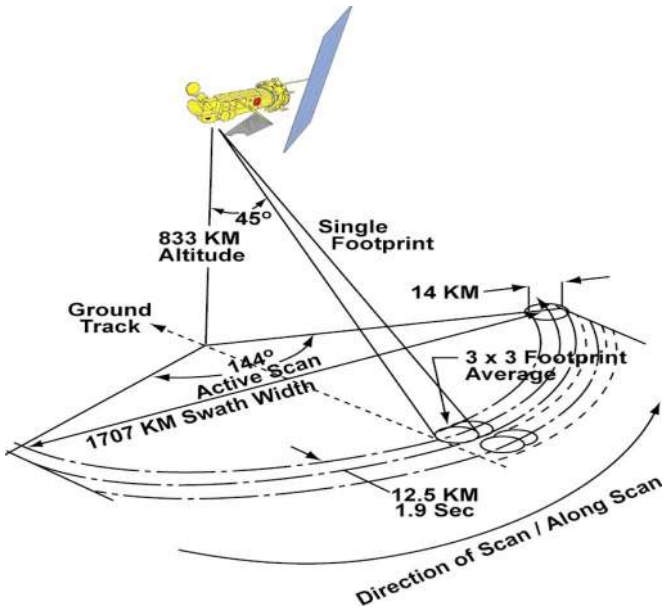

Fig. 2. SSMIS scan geometry showing direction of active scan, swath width, ground track, and footprint averages.

six feedhorns, a broadband warm-load calibration target, and a small reflector pointed toward the cosmic background, providing a cold-space calibration target. The main reflector, a lightweight graphite/epoxy offset parabolic laminate shell with a diameter of 0.6096 m and $f/D = 0.3846$, is illuminated by six broadband corrugated feedhorns, resulting in frequency multiplexing in terms of Channels 1–5; Channels 6, 7, 19–24; Channels 12–14; Channels 15–16; Channels 8–11; and Channels 17–18. The main and cold-space reflector surfaces have vacuum deposited coatings of aluminum and silicon oxide to obtain high reflectivity at microwave frequencies and prevent large on-orbit temperatures under solar illumination.

The antenna feeds are positioned in the reflector focal plane to produce centroids of the secondary antenna beams that trace the same one-half cone angle, 45°, with respect to the local spacecraft zenith. The instrument spins in the counterclockwise direction about the spacecraft zenith with a spin rate of 31.6 r/min that provides approximate contiguity of the projected along-track 3-dB contours on the Earth's surface of the highest resolution antenna beams (Channels 8–11 and 17–18; Fig. 5). (For reference, 3-dB contours of the SSM/I beams, displaced

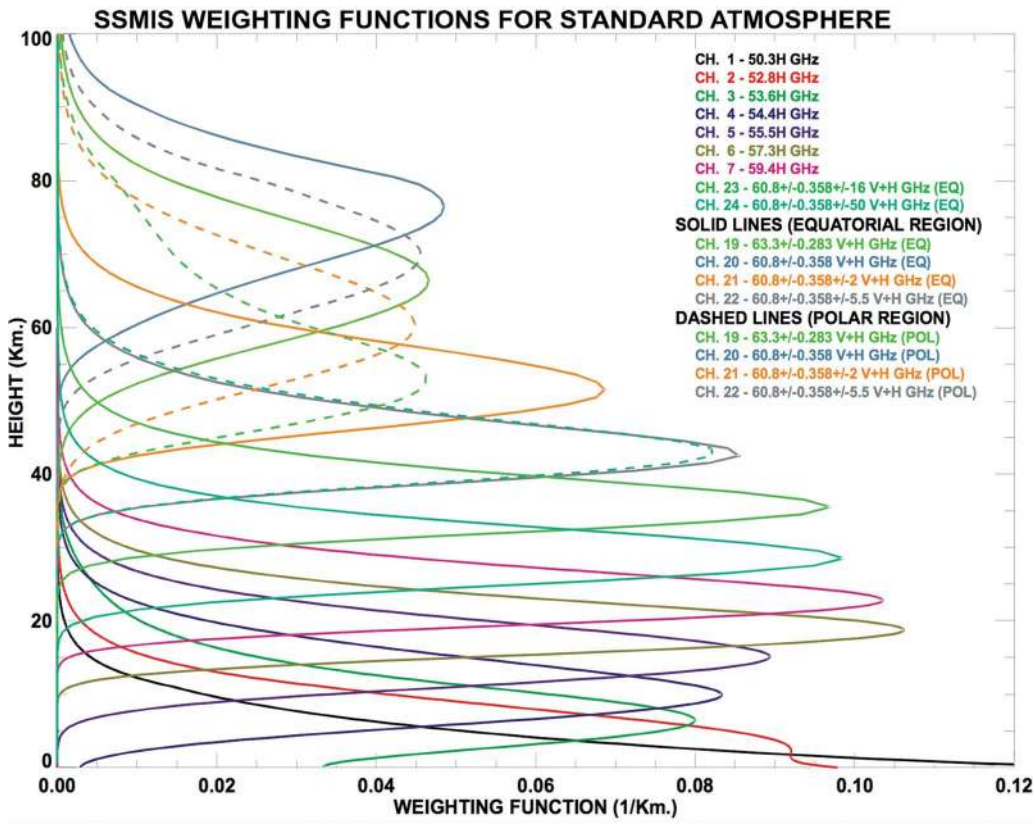

Fig. 3. SSMIS weighting functions for standard atmosphere.

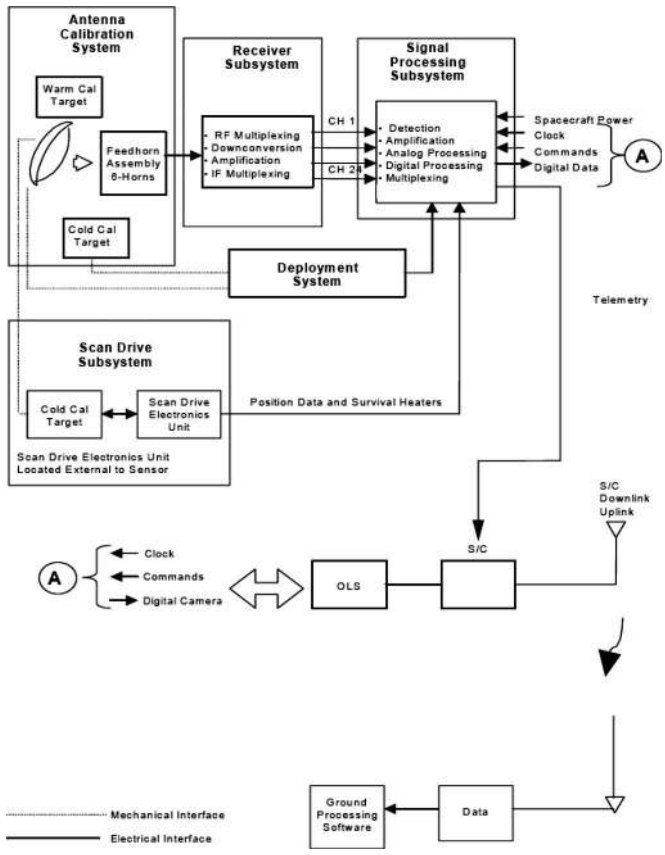

Fig. 4. SSMIS simplified block diagram.

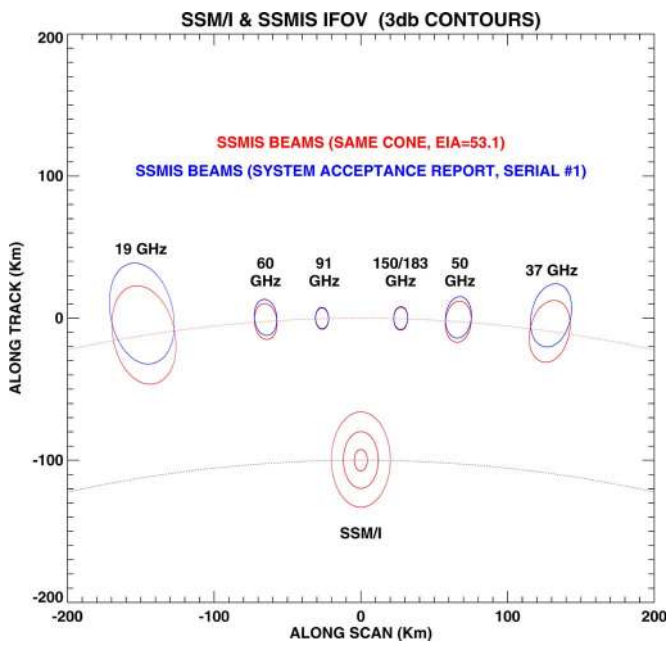

Fig. 5. SSM/I and SSMIS instantaneous FOV (IFOV) 3-dB contours.

in along-track direction, are included.) The projection of the instantaneous 3-dB antenna contours onto the Earth's surface from a 840-km satellite altitude produces ellipses with nominal dimensions (in kilometers): 17 × 29 for Channels 1–5; 16 × 26 for Channels 6, 7, and 19–24; 9 × 15 for Channels 8–11,

17, and 18; 44 × 72 for Channels 12–14; and 26 × 44 for Channels 15–16. All channels are sampled every scan, and a fixed receiver integration time of 4.1 ms and a sampling period of 4.22 ms (corresponding to 0.8° azimuth scan increment) are used for each channel. These samples are, in turn, subjected to onboard flight software averaging in the along-scan direction to improve the noise-equivalent difference temperature (NEDT),[1] meet the instrument data rate of 14.22 kb/s, and produce 60 uniformly spaced samples per scan for Channels 1–7; 180 for Channels 8–11 and 17–18; 90 for Channels 12–16; and 30 for Channels 19–24. Antenna beam registration of all channels along with an additional beam averaging is performed in the Ground Data Processing Software (GDPS) to obtain nearly circular concentric antenna beams in the along-track and along-scan directions and further reduction in the NEDT of the scene samples (Table I).

For each scan, the feedhorns pass beneath the stationary warm-load and cold-space reflector calibration targets, interrupting the FOV of the feedhorn to the main reflector and providing, with the exception of the main reflector, an end-to-end periodic radiometric calibration of the instrument. Four samples of each calibration target are taken each scan for all channels, averaged by the onboard flight software and downlinked to the GDPS. The warm load is a well-matched broadband microwave load composed of tapered pyramids coated with a magnetically loaded microwave absorbing material. Its temperature is maintained at a nominal 302 K with periodic measurements by three high-precision platinum-resistive temperature probes.

The receiver subsystem accepts the energy from the six antenna feeds and provides amplification, filtering, and additional frequency multiplexing to output 24 discrete frequency bands to the signal processing subsystem. The 19-, 22-, and 37-GHz channels are implemented as direct detection receivers with the incoming energy amplified by low-noise amplifiers and directly detected at the microwave frequency without frequency downconversion as required in conventional superheterodyne receivers. This approach eliminates the need for a local oscillator (LO), mixer, and intermediate amplifier, resulting in minimum hardware, weight and power, and improved NEDT.

The 50–60-, 91-, 150-, and 183-GHz channels are implemented in the more conventional superheterodyne configuration. The 150- and 183-GHz channels utilize proprietary subharmonically pumped mixers developed by NGES with LOs operating at one-half the signal frequency. Improved NEDT performance is achieved for Channels 1–7 and 19–24 by employing low-noise amplifiers before downconversion of the upper sidebands. Channels 19–24 pose several unique receiver design challenges. These channels operate near the peak of the oxygen absorption region and require very narrow passbands, tight frequency stability, and low-noise performance. For example, the frequency stability requirement for these channels is typically 100 kHz at 60 GHz compared to the less stringent requirement of 10 MHz for the lower air sounding Channels 1–7 (Table I).

The high-frequency stability is achieved using a millimeter-wave oscillator that is locked to a low-frequency oven-controlled crystal oscillator and ultrastable surface acoustic wave (SAW) filters for intermediate frequency (IF) channelization. Implementation of the SAW devices requires that these channels use a double-frequency downconversion to place the IF passbands in the optimum operating frequency range of the filters. A unique frequency calibrator is used to maintain a long-term frequency stability of the tunable oscillator. Due to the extremely narrow passbands, another design challenge arises from having to compensate for significant Doppler shift due to the motion of the spacecraft relative to the received upwelling scene energy incident on the antenna. Since the Doppler shift of the received scene energy can be expressed in terms of the known antenna scan position and spacecraft velocity, a dynamic correction is made by changing the LO frequency in accordance with the Doppler shift. The tuning signal for the LO is generated in the signal processing subsystem and synchronized to the sensor azimuthal scan position.

The integrated outputs of the 24 channels are digitized using a 16-bit analog-to-digital converter along with various support/housekeeping data that include temperatures of the receiver shelves, power supply components, phase-locked loop oscillators, reflector support structure, radiator panels, and currents and voltages of key components. The digital processor uses a CPU with control through processing functions contained in the uplinked flight software. An essential function of the flight software is to compress the 16-bit data to 12 bits using the average warm and cold-space calibration radiometric observations to insure that the data rate is compatible with the maximum allowable data rate, i.e., 14.22 kb/s. The processor uses a fully redundant CPU, memory, and analog-to-digital converter, whereas secondary sensor power is provided by partially redundant components.

The scan drive subsystem consists of an assembly mounted in the sensor and the drive electronics mounted external to the sensor. The drive assembly provides the mechanical interface between the rotating sensor and its fixed mount and consists of a motor, position encoder, and slip rings. The slip rings are used to transmit power and signals between the stationary and rotating portions of the sensor. The scan drive electronics controls the sensor spin rate to within 0.05%. The scan drive subsystem is fully redundant except for the motor.

The deployment subsystem consists of three separate deployments: rotation of the main reflector, rotation of the cold-space reflector, and the main sensor body. The main sensor body deployment consists of a 90° rotation and 26.38 cm (10.387 in) translation of the sensor body away from the spacecraft. The main sensor deployment also acts as the caging subsystem to secure the sensor in its stowed configuration during launch. The structural/thermal subsystem consists of the canister structure that houses all other subsystems, instrument temperature sensors, thermal control surfaces, and heaters. The thermal design is a cold bias configuration with radiated area and active heater power to provide temperature margins over the range of expected orbital conditions.

[1]Within this paper, NEDT can be interpreted as the minimum change in system noise necessary to produce a detectable change at the radiometer output (ΔT_{SYS}) [3].

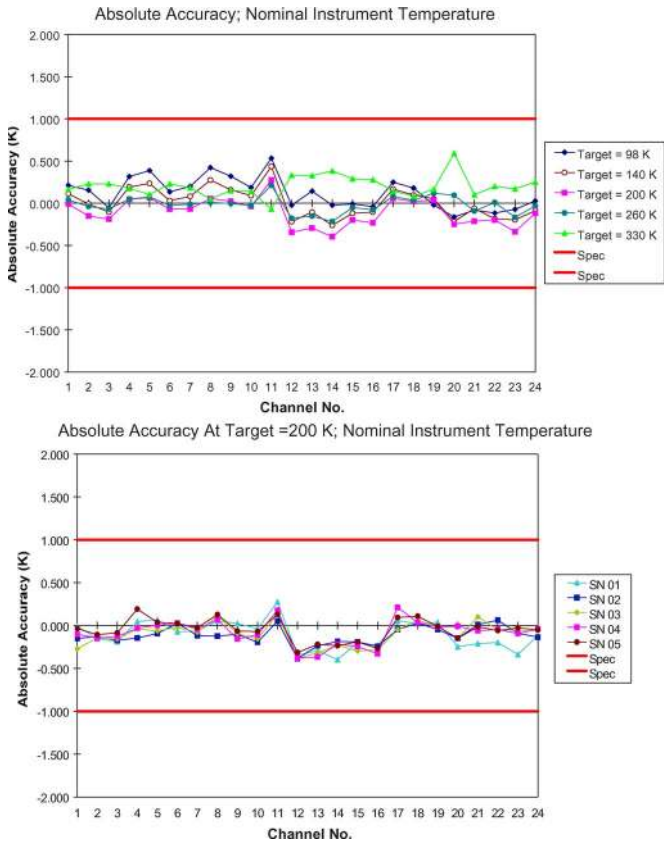

Fig. 6. SSMIS prelaunch calibration accuracy. (a) S/N 02 (on F-16). (b) All instruments for calibration target at 200 K. (Calibration accuracy is specified as the difference between the radiometer observed temperature referenced to the waveform input to the feedhorn and the average thermometric temperature of the target.)

Special laboratory temperature-controlled radiometer calibration targets were developed to provide high-temperature stability over extended calibration periods for target temperatures between ∼100 and 330 K. The extrapolation of the thermal vacuum calibration results based on 100-K cold target to on-orbit cosmic background cold calibration reference of 2.7 K is made on the basis of the high degree of linearity required in the receiver square-law detectors and amplifiers, typically better than one part in 100 000.

Representative SSMIS Thermal/Vacuum (T/V) radiometer calibration performance results (without the main reflector and cold-space reflector target replaced by a liquid-nitrogen-cooled calibration target) are presented in Fig. 6, for nominal instrument operating temperature. Calibration accuracies are shown for all five SSMIS instruments identified by a serial number (F-16 is SN 02) for a range of target temperatures from 98 to 330 K and meet the prelaunch calibration accuracy requirement of 1 K with considerable margin.

To facilitate the transition of SSMIS EDR products to users, the DMSP office in conjunction with the Space and Naval Warfare Systems (SPAWAR) initiated a comprehensive end-to-end calibration (instrument level) and validation (EDR level) of the first SSMIS. The Naval Research Laboratory (NRL) was selected to lead the technical efforts of the calibration/validation (cal/val) with support from remote sensing scientists and sensor experts from The Aerospace Corporation. The Air Force Weather Agency (AFWA) and the Fleet Numerical Meteorology and Oceanography Center (FNMOC) provided SSMIS data processing and validation data and with NRL and Aerospace comprising the core cal/val team. Additional support was provided by the instrument manufacturer. The remainder of this paper presents a summary of the major results of the SSMIS cal/val program, including both sensor-related performance as well as EDR results.

III. SSMIS Cal/Val

The SSMIS cal/val effort was designed to: 1) verify the end-to-end instrument radiometric performance including long- and short-term stability, NEDT, and absolute calibration accuracy and 2) validate the Imaging and Sounding EDRs for the needs of the DMSP mission and data users. To accomplish these goals, cal/val activities followed the path shown in Fig. 7. Due to the diverse aspects of ensuring data product quality, a successful cal/val requires investigation of several potential error sources that lie not only in the on-orbit observations but also in the ground truth, and the Temperature Data Record (TDR), Sensor Data Record (SDR), and EDR processing. A key aspect of these activities is the ability to bring together many diverse sources of data with a thorough understanding of its utility and limits of validity.

A. Cal/Val Objectives and Process

As suggested in Fig. 8, errors associated directly with the space-based observations include many aspects of the sensor that require detailed prelaunch characterization such as antenna spillover, cross-polarization coupling, beam pointing, frequency stability, and passband response. Several of these potential error sources may not be completely understood or may have significant uncertainties in their prelaunch characterization. Accordingly, application of prelaunch sensor characterization coefficients such as beam spillover and calibration correction coefficients may only marginally improve performance or even encourage misleading conclusions in error analyses and root-cause investigations. Uncertainty and errors in prelaunch sensor characterization coefficients may arise from the "low contrast" prelaunch background environment; that is, the cold on-orbit background is extremely difficult to simulate on the ground or in a laboratory where the background "scene" is typically near the same temperature as the sensor and warm load, rather than the cold target temperature. Therefore, many carefully-measured prelaunch coefficients designed to improve performance of space-based radiometers need to be revalidated or rederived on-orbit.

Another aspect of the postlaunch cal/val is the limited available insight regarding root-cause and error analysis. For example, an error caused by nonlinearity may be incorrectly treated as an error associated with a calibration target unless the investigator has extensive experience and insight regarding the entire radiometer system along with sufficient on-orbit "housekeeping" and truth data to determine the correct conclusion. Another example can be found directly in the SSMIS cal/val experience with microwave reflector emission. Precision

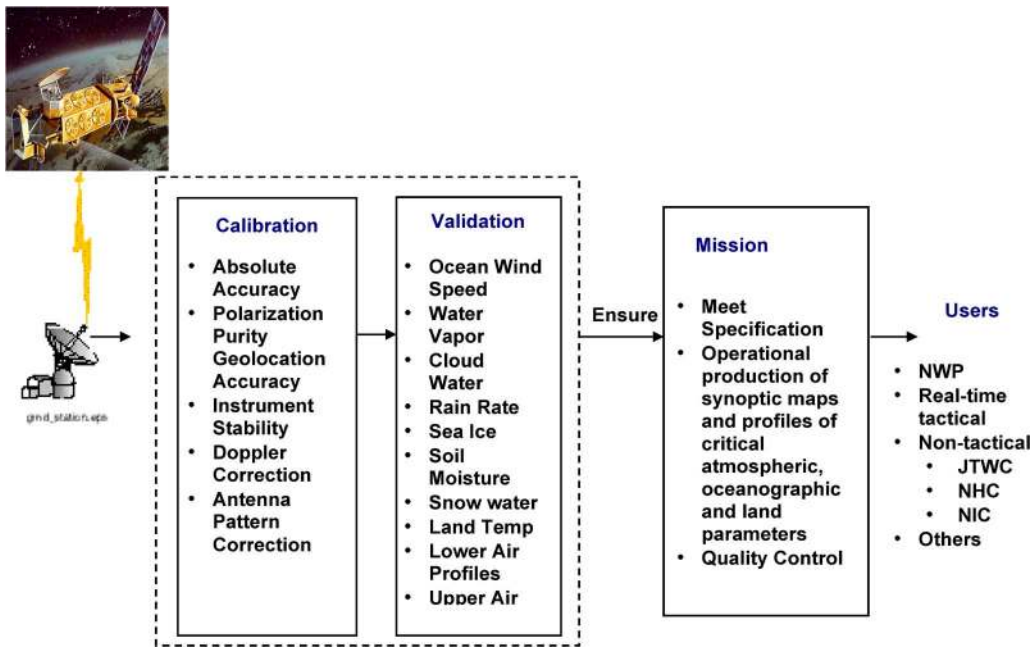

Fig. 7. Process and purpose of SSMIS cal/val effort separately showing components of the cal/val phase in relation to the mission expectations and data users.

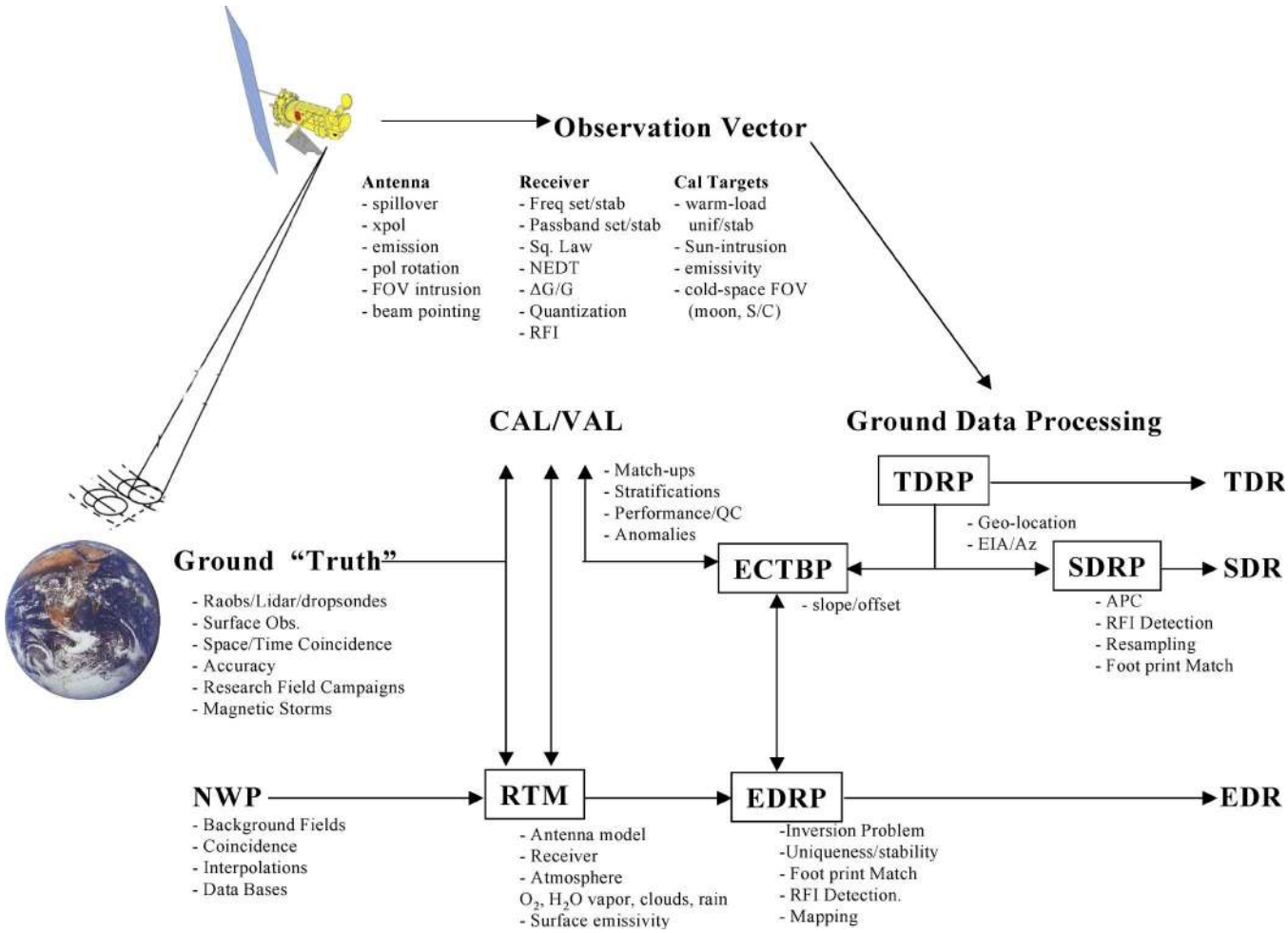

Fig. 8. Origination of uncertainties and errors in the cal/val process of space-based microwave sensors. Error sources in the on-orbit brightness temperature measurements, ground truth, aspects of NWP models, RTM, TDRP, SDR Processor (SDRP), EDR Processor (EDRP), and Empirically Corrected Brightness Temperature Processor (ECTBP) are listed.

matchup data at a single location revealed only that a systematic bias was occurring during certain times of the year. However, it was not until comparisons were made between global NWP fields and a detailed graphic simulation of the SSMIS sensor on-orbit that it became clear that thermal emission coupled with large temperature swings of the main reflector was the likely explanation of the systematic biases observed earlier in the matchup data. In retrospect, it was clear. Our conclusion is that careful multiperspective analyses enabled by the availability of many sources of data are essential to the cal/val of precision state-of-the-art on-orbit sensors. The SSMIS cal/val elucidated precision characteristics of the sensor in order to evaluate the accuracy of warm-load correction coefficients, Doppler calibration correction coefficients, and scan-position-dependent biases to a sub-Kelvin level that had not been seen before with this type of radiometer in-orbit. The SSMIS cal/val also identified solar intrusion into the SSMIS warm load that in turn initiated an investigation into SSM/I data revealing the same effect had been occurring over a decade earlier and had not been previously known (see Section IV-E). With adequate preparation and proper analysis tools in place prior to launch, the cal/val is the first opportunity to assess and quickly correct sensor operation as well as to provide timely and essential lessons learned for the next generation of sensors under development.

B. SSMIS Cal/Val Plan

Following the above approach, the SSMIS cal/val involved multiple agencies, each contributing in a key fashion: NRL provided sensor science and engineering support with extensive numerical sensor performance characterization software tools, Aerospace provided support for ground data processing, LIDAR truth data, and DMSP graphic simulation tools, and the European Center for Medium-range Weather Forecasts (ECMWF) working through NRL provided background NWP fields for SDR assessment. The SSMIS cal/val plan consisted of five components: 1) early-orbit evaluation; 2) initial assessment; 3) system calibration; 4) EDR validation; and 5) algorithm improvement [2]. As a result of following this plan, several changes were made in the SSMIS GDPS to correct for geolocation errors [4], FOV intrusions [5], calibration anomalies [6], [7], and channel polarization errors [8] in order to provide quality flagged and validated SSMIS SDRs and EDRs to operational users. Second, several new aspects of the SSMIS (and SSM/I) sensor operation were discovered and a more complete understanding of calibration errors established providing a basis for future improvements to SSMIS data quality.

C. Cal/Val Techniques for SSMIS

Early-orbit evaluation of the SSMIS is facilitated by special instrument operating modes developed to assess fundamental aspects of sensor operation upon successful launch, deployment, and sensor spin up. These modes, called the early-orbit modes, are very important for the SSMIS since they provide the only opportunity to examine the individual warm-load and cold-space calibration samples and to directly assess potential FOV intrusion effects. This cannot be done in the sensor's normal mode because the individual calibration samples are not available; the SSMIS flight software performs an onboard data average of the last eight scans of four fixed calibration samples from each target. Further, there is substantial along-scan averaging and data processing that cannot be disabled in normal mode. Therefore, early-orbit modes are required in order to directly evaluate data sampled from every scan position of the SSMIS.

The SSMIS was powered on, deployed, and commanded to begin spinning approximately one week after launch. An initial assessment of the SSMIS radiometric operation, sensitivity, calibration, and stability was then performed. During this phase, the initial assessment of the SSMIS imaging SDRs and EDRs relied on SDR images, cumulative brightness temperature statistics, comparisons between ascending and descending phases of the orbit, trending over the full Earth scene FOV, and comparisons with corresponding SSM/I parameters. In support of these comparisons, the SSMIS housekeeping data, including temperature sensors dedicated to each of the six receiver plates, were used to evaluate the manner in which the sensor responds to its ambient environment.

Geolocation analyses were performed using shoreline extraction and imaging techniques to resolve any needed elevation and azimuthal corrections in beam pointing. Geolocation errors in excess of 20–35 km were detected in the imagery by superimposing accurate global shoreline databases. Image analysis tools were developed to extract the sensor shoreline map in both the along-scan and along-track directions and allow the quantification of the angular offset of the sensor spin axis and misalignment to the spacecraft. Systematic offsets in pitch and yaw were developed and implemented in the geolocation algorithm in the ground processing software to bring the residual geolocation errors within requirements.

Limited analyses of coincident buoy data with LIDAR and Radiosonde Observation (RAOB) matchups were carried out to elucidate systematic errors in the sensor calibration. Comparisons with NWP fields were also arranged for the SSMIS cal/val and found to be very valuable for identifying calibration anomalies associated with the warm load and antenna reflector as described in the next section.

Underflights were performed with the Airborne Polarimetric Microwave Imaging Radiometer (APMIR) [9], [10] and the Conical Scanning Microwave Imaging Radiometer (CoSMIR) [8]. These flights provided two additional independent bases for assessing the SSMIS calibration. During the cal/val, the CoSMIR instrument helped to identify a design flaw in the F-16 SSMIS; S/N 02 Channels 1–5 measure V-pol instead of H-pol as designed. As a result of uncovering significant calibration anomalies (2–5 K depending on the channel) and the incorrect sensor polarization, analyses were initiated within the Government and Northrop-Grumman teams during the cal/val to support development of mitigation algorithms in the ground-based algorithms.

Although the F-16 SSMIS was found to exhibit on-orbit transient calibration anomalies (see Section IV), the errors did not prevent a thorough analysis of the SSMIS EDR performance during the cal/val. As described in Section V, the SSMIS is able to provide data comparable to SSM/I in nearly all cases

TABLE II
WARM-LOAD NEDT VALUES FROM THE SSMIS CAL/ VAL SHOWING MEAN VALUES FOR A SAMPLE OF ORBITS RANGING FROM ORBIT 518 (NOVEMBER 29, 2003) TO ORBIT 10538 (NOVEMBER 2, 2005)

Channel	Orbit 518	Orbit 1718	Orbit 2918	Orbit 4399	Orbit 5728	Orbit 7994	Orbit 8500	Orbit 9500	Orbit 10200	Orbit 10538	T/V Recal	Spec.
1	0.21	0.19	0.21	0.18	0.20	0.22	0.19	0.21	0.24	0.20	0.19	0.40
2	0.21	0.21	0.18	0.18	0.20	0.24	0.20	0.19	0.24	0.20	0.19	0.40
3	0.21	0.19	0.19	0.19	0.21	0.24	0.19	0.20	0.21	0.20	0.19	0.40
4	0.22	0.20	0.19	0.19	0.21	0.20	0.21	0.19	0.20	0.22	0.20	0.40
5	0.25	0.22	0.22	0.20	0.24	0.22	0.23	0.21	0.24	0.20	0.22	0.40
6	0.28	0.28	0.27	0.27	0.28	0.28	0.29	0.28	0.27	0.25	0.28	0.50
7	0.34	0.32	0.30	0.33	0.33	0.32	0.32	0.34	0.34	0.34	0.32	0.60
8	0.52	0.52	0.47	0.49	0.54	0.45	0.51	0.52	0.49	0.54	0.40	0.88
9	0.66	0.67	0.69	0.69	0.69	0.59	0.65	0.70	0.63	0.71	0.59	1.20
10	0.60	0.64	0.60	0.61	0.63	0.66	0.65	0.65	0.63	0.63	0.54	1.00
11	0.83	0.86	0.88	0.91	0.85	0.86	0.87	0.88	0.90	0.93	0.74	1.25
12	0.38	0.31	0.37	0.37	0.34	0.35	0.35	0.35	0.37	0.37	0.32	0.70
13	0.49	0.47	0.46	0.48	0.47	0.46	0.48	0.49	0.51	0.45	0.42	0.70
14	0.40	0.36	0.45	0.38	0.39	0.40	0.40	0.40	0.39	0.40	0.37	0.70
15 *	0.40	0.32	0.37	0.37	0.35	0.99	2.96	1.46	1.26	0.37	0.28	0.50
16	0.32	0.27	0.28	0.29	0.27	0.29	0.29	0.27	0.28	0.31	0.22	0.50
17	0.21	0.21	0.21	0.20	0.20	0.19	0.20	0.21	0.21	0.21	0.16	0.30
18	0.28	0.28	0.31	0.27	0.31	0.49	0.57	0.44	0.43	0.46	0.25	0.30
19	1.49	1.34	1.28	1.37	1.33	1.36	1.38	1.24	1.43	1.33	1.42	2.38
20	1.35	1.21	1.40	1.28	1.30	1.30	1.29	1.33	1.20	1.43	1.43	2.38
21	1.01	0.94	1.03	0.93	0.98	1.13	0.98	0.93	1.16	1.02	1.05	1.75
22	0.66	0.64	0.69	0.72	0.67	0.72	0.70	0.63	0.66	0.71	0.75	1.00
23	0.44	0.42	0.40	0.36	0.39	0.47	0.42	0.43	0.48	0.40	0.43	0.60
24	0.23	0.24	0.23	0.22	0.21	0.33	0.23	0.22	0.34	0.21	0.23	0.35

* The computed NEDT for channel 15 contains anomalous intermittent orbital receiver gain changes starting Jan 05. These changes do not affect scene SDRs due to periodic warm and cold space calibration

involving heritage surface algorithms. For sounding and NWP applications, the sensor calibration anomalies become much more important and may ultimately limit the utility of the SSMIS for these applications unless an effective mitigation strategy can be determined and applied to the data. The next two sections describe the SDR and EDR performance evaluation from the DMSP F-16 SSMIS cal/val.

IV. SDR PERFORMANCE ANALYSIS

The SSMIS cal/val period began upon the F-16 launch and was completed on schedule 18 months after launch, on April 27, 2005, with the release of validated EDRs and a stable configuration of the sensor and ground processing software. Analysis and characterization of SSMIS SDR and EDR data continued through development of the cal/val final report, completed on November 30, 2005. The SSMIS radiometric sensitivity (NEDT), initial geolocation accuracy, Earth scene FOV, and intersensor calibration were established in the sensor calibration phase of the cal/val.

A. Radiometric Sensitivity

The sensor NEDT values were collected and found to be very stable over the entire cal/val and report formulation period (October 2003–November 2005) and consistent with prelaunch T/V, as shown in Table II. As seen in the table, Channel 15 is the only channel that has shown significant variability in the NEDT due to an intermittent and temperature-dependent RF gain anomaly. The gain changes in discrete steps infrequently (typically no more than twice per orbit) with respect to the SSMIS calibration cycle that occurs for every scan; therefore, radiometric calibration of this channel is essentially unaffected.

The mean receiver plate temperatures for Channels 12–14 and 15–16 over the two-year data collection period are typically $\sim 15 \pm 0.5$ °C, and the plate temperatures for Channels 1–5 and Channels 6, 7, and 19–24 are typically each < 0.25 °C lower. The mean receiver plate temperature for Channels 8–11 is typically ~ 0.6 °C warmer than Channels 12–16. The receiver plate for Channels 17–18 is colocated with a pulsewidth-modulated heater that maintains the plate under nominal conditions to 16.5 ± 0.1 °C. The interorbit variability for all receiver plate temperatures is typically < 2 °C. Because of the active thermal control within the receiver bay and its stabilizing effect on all receiver plates, the SSMIS radiometers were not designed to have active gain control. The on-orbit data validate the design, showing very stable system noise temperatures from the SSMIS radiometer suites.

B. Geolocation

Objectives of the sensor calibration portion of the cal/val included quantification of geolocation errors and then establishment of geolocation accuracy to within the requirement of a $\leq$ 7-km error. To derive geolocation errors, radiometric data were overlaid with shoreline databases in 15 specific regions over the globe. The data were further subdivided according to: 1) ascending and descending passes; 2) along-track and cross-track scan regions; and 3) scan start time offset. The SSMIS geolocation error analysis also involved repeatability and stability assessments, and resampling to adjust data to a common SDR grid. Analysis of pointing and time-related errors was

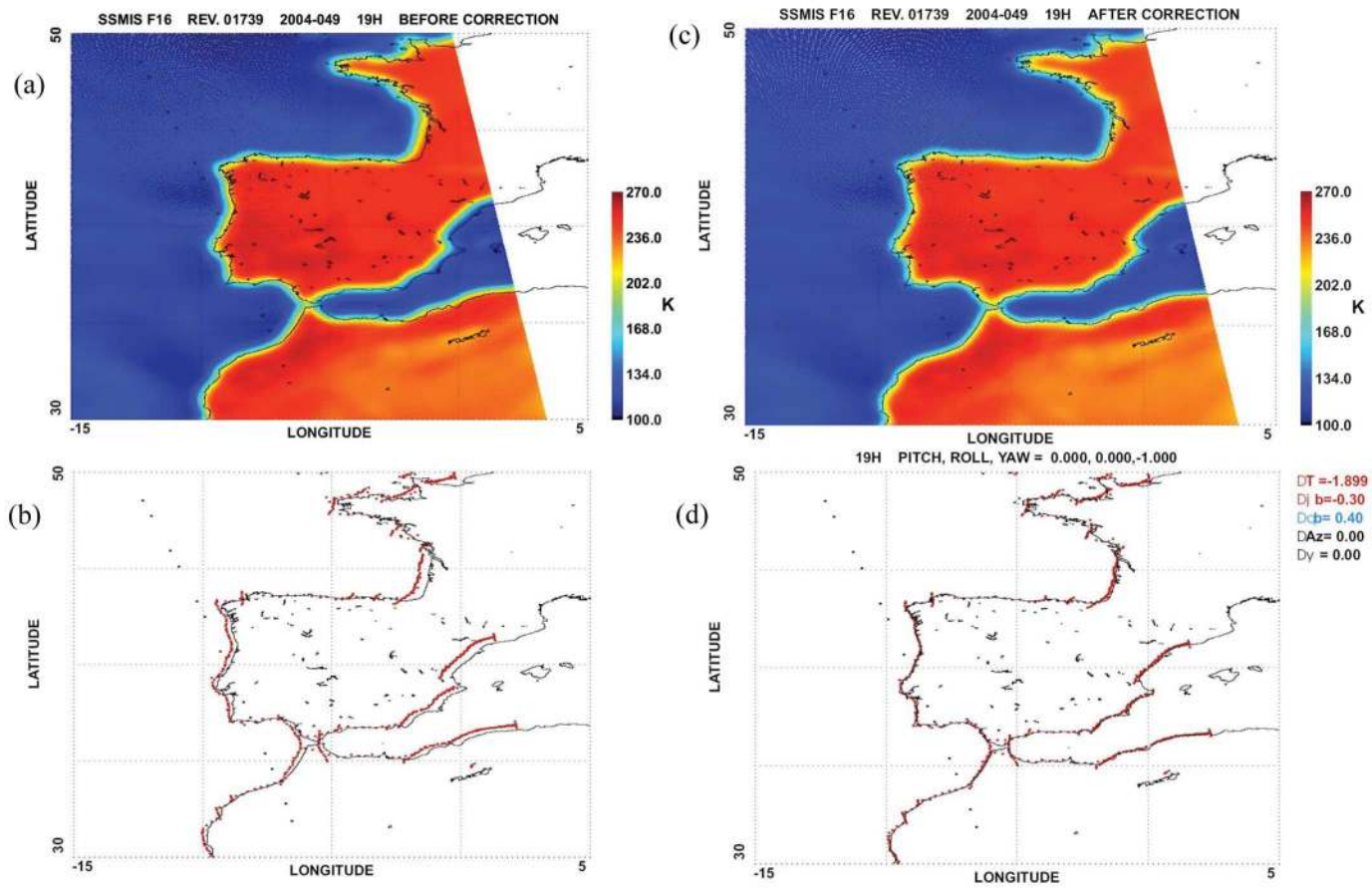

Fig. 9. (Left insets) Geolocation performance for Channel 12 before and (right insets) after angular beam offset corrections. Top figures show individual pixel samples superimposed on the global shoreline database. Red lines in bottom figures show the along-scan shoreline extracted from radiometer imagery, whereas blue lines show the along-track shoreline.

needed for each SSMIS antenna feed due to the individual feed offsets. Because none of the upper atmospheric sounding (UAS) channels (6, 7, 19–24) view the Earth's surface, geolocation errors were inferred for these channels.

The SSMIS was found to have initial geolocation errors in excess of the 7-km requirement [Fig. 9(a) and (b)]. During the course of the cal/val, these errors were attributed to a common yaw offset of -1.0° and -1.899-s time ($\sim$1 scan) error, individual antenna beam offsets of 0.4° elevation and -0.3° azimuth for Channels 12–14, and -0.2° elevation and 0° azimuth for Channels 8–11, and 17–18. After correction of these errors in the GDPS, geolocation errors were found to be stable and $\leq$ 6 km [Fig. 9(c) and (d)]. Further details on the geolocation analyses and corrections for the F-16 SSMIS can be found in [4].

C. Sensor FOV

Correct alignment of the warm and cold calibration target locations was verified using early-orbit mode data to collect samples from all scan positions in the vicinity of the calibration targets. Results from the early-orbit mode data collection indicated that the two calibration standards appeared as expected, with uniform values within the calibration sample region used for normal mode. Indeed, it is apparent that additional calibration samples could be included in the calibration to lower the cumulative calibration sample noise without introducing calibration biases. Data from Channel 12, having the widest antenna feed footprint on the warm load, indicated that the number of calibration samples could be doubled to 8 from 4. A similar observation occurred for the cold-sky observations in Channel 12 suggesting that up to $\sim$16 samples, each with an identical value to within $\sim$0.05 K, could be used for calibration each scan. Other channels showed similar behavior; however, changes to the sensor calibration approach were not made during the cal/val. Details of the early-orbit mode FOV analysis performed during the SSMIS cal/val can be found in [5].

The Earth scene FOV was examined using early-orbit and normal mode data. For the early-orbit mode, "raw A/D counts" were calibrated to radiometric brightness temperatures manually using warm-load and cold-sky target brightness temperatures from the same scan positions used in normal mode. Normal mode data were collected over $\sim$12-month period to reduce the scene-dependent variability and derive a stable mean value for each scan position within the Earth scene FOV. The goal for normal mode data collection applied to FOV analysis was to achieve a highly stable estimate of average scene brightness temperature at each scan position. For data collection in the early-orbit mode, only a few orbits of data

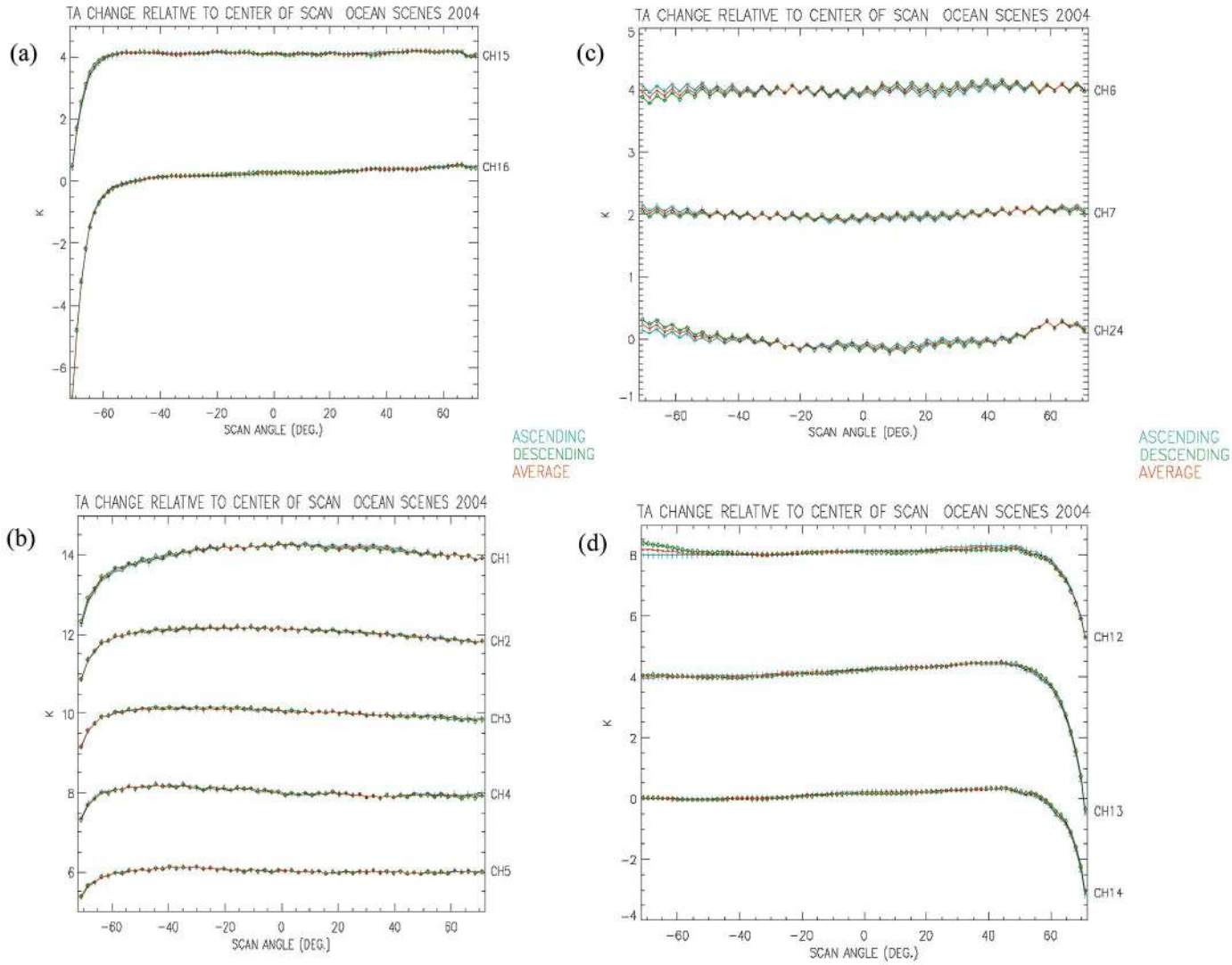

Fig. 10. Twelve-month averaged brightness temperatures shown as a function of scan position in normal mode. The scan progresses in a counterclockwise fashion so that the start of scan is represented by scan angle $+72^\circ$ and the end of scan is at scan angle -72°. (a) Channels 15–16. (b) Channels 1–5. (c) Channels 6, 7, and 24. (d) Channels 12–14.

could be collected; however, early-orbit data provided raw counts with no additional data processing onboard or in the GDPS. Therefore, consistency between early-orbit and normal mode data was a good check for sensor or geophysical biases in the data sets.

Examination of the along-scan scene brightness temperatures for Channels 15–16 indicates rapid decreases near end of scan of $\sim$3.5 and $\sim$7.3 K [Fig. 10(a)]. This has been attributed to an FOV intrusion to the antenna feed from the warm-load cover and associated multilayer insulation (MLI) placed over the warm load to control its thermal characteristics. A similar impact to Channels 1–5 brightness temperatures at the end-of-scan is also attributed to the warm load and MLI covering [Fig. 10(b)]. Additional calibration error attributed to the Doppler correction scheme is also present in the sounding channels 1–7 and 19–24 [5]. A physical optics electromagnetic model of the antenna and its FOV indicated no impact from any potential blockages external to the SSMIS for any channel.

Twelve-month averaged brightness temperatures from Channels 8–11 and 17–18 show very uniform behavior as a function of scan position. Because the associated antenna feeds are at the center of the feed assembly, minimal edge of scan bias is expected. Similarly, averaged brightness temperatures from Channels 6 and 7 are relatively flat across the swath, whereas Channel 24 shows a small $\pm$0.2–0.3 K variation across the scan attributable to the Doppler correction scheme [Fig. 10(c)]. In contrast to the end of scan bias observed with Channels 15–16, a beginning of scan bias is found to be $\sim$2.7 K for Channel 12, $\sim$4.7 K for Channel 13, and $\sim$3.0 K for Channel 14 [Fig. 10(d)]. These biases have been attributed to intrusions of the Channel 12–14 antenna feed FOV by the cold-sky reflector [5].

All scan-dependent biases discussed in this section were corrected in the TDR Processor (TDRP) by deriving the FOV from on-orbit data. Thus, we have

$$T_A(\phi) = L(\phi) T_{\text{Scene}} + [1 - L(\phi)]\, T_X \tag{1}$$

where $T_A(\phi)$ is the antenna temperature as a function of azimuth scan angle, and T_X is the cosmic background brightness temperature. Since $|1 - L| \ll 1$

$$T_{\text{Scene}} \approx \frac{T_A(\phi)}{L(\phi)} \tag{2}$$

$$L(\phi) = \frac{\langle T_A(\phi) \rangle}{\langle T_A(\phi : \text{Center}) \rangle}. \tag{3}$$

After applying (3), scan uniformity appears stable and uniform across the swath to within ~0.1–0.2 K.

D. SSM/I SDR Comparisons

Cross-calibration mapping of the F-16 SSMIS (LTAN 19:54) to the F-14 SSM/I (LTAN 19:26) was performed to evaluate the SSMIS SDR absolute calibration and prepare for EDR retrieval comparisons in the validation phase of the cal/val, i.e.,

$$\hat{T}_P = f(T_P) = mT_P + b \tag{4}$$

where $\hat{T}_P$ is the F-16 SSMIS brightness temperature measurement mapped to an 'equivalent' F-14 SSM/I brightness temperature, and T_P is the measured F-16 SSMIS brightness temperature. The mapping addresses biases arising from: 1) EIA differences, primarily in Channels 12–14; 2) antenna spillover; 3) channel frequency, primarily in Channels 17–18; 4) warm-load and cold-sky target biases; and 5) channel bandwidths. The SSM/I SDR processing includes: 1) corrections for the SSM/I scan nonuniformity; 2) antenna pattern correction, addressing cross polarization and spillover; and 3) solar intrusion into warm-load correction.[2] The SSMIS SDR calibration includes corrections of solar-contaminated warm-load calibration samples discussed in the following section.

The slope and offset in (4) are selected to minimize the following:

$$\varepsilon^2(m, b) = \frac{1}{N} \sum_{k=1}^{N} [S_P(k) - b - mT_P(k)]^2 \tag{5}$$

where N is the number of SSM/I–SSMIS matchups, $S_P(k)$ is the SSM/I SDR of channel P and matchup k, and $T_P(k)$ is the respective SSMIS SDR. The slope and offset are unique for major surface types: 1) ocean; 2) land; and 3) sea ice, all under rain-free conditions established by the SSM/I rain flag. Matchup data from November 6, 2003 were used as the development set and test sets from January 14, 2004 and March 23, 2004 are included in the difference distributions shown in Fig. 11. In general, good statistical agreement is obtained between the F-14 and F-16 matchup tests. It should be noted that adding nonlinear terms to (4) resulted in minor reduction of the mean squared difference (5).

[2]This correction to the SSM/I calibration was determined as part of the SSMIS cal/val when it was discovered that solar intrusions to the SSMIS warm load were responsible for calibration anomalies.

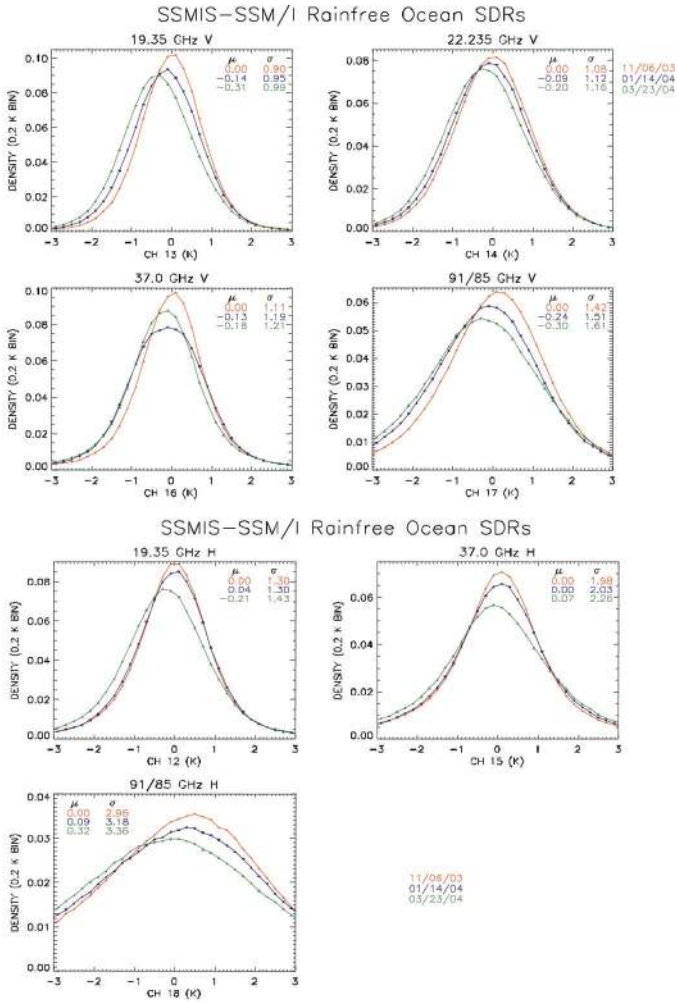

Fig. 11. Cross-calibration difference distributions of SSM/I and SSMIS SDRS for rain-free ocean scenes. The data in red from November 6, 2003 are the development set showing no residual mean offset as expected. Test sets from January and March 2004 show general consistency but SSMIS values decreasing slightly relative to SSM/I with time.

E. Warm-Load Solar Intrusions

During the cal/val period, it was discovered that solar intrusions onto the warm-load absorbing surface were biasing the SSMIS calibration typically three or four times every orbit for as much as several minutes at a time [6], [7] [Fig. 12(a)]. The impact was a temporary negative SDR bias of < 1 to ~3 K, depending on the local time of day, typically, but not exclusively, in the descending phase of the orbit.

To facilitate evaluation of the absolute calibration accuracy of the SSMIS surface channels, characterize the solar intrusions, and determine an effective mitigation technique, a best-fit calibration function for each SSMIS surface channel was designed based on Fourier analysis of the low-frequency filtered time-varying radiometric gain function over a series of three orbits. These orbits were chosen to maximize the number of matchups with the DMSP F-14 orbit carrying SSM/I. In this manner, a high-quality intersensor comparison and calibration difference evaluation of the SSMIS could be performed as described above in (5). The filtering process of SSMIS channel gains was

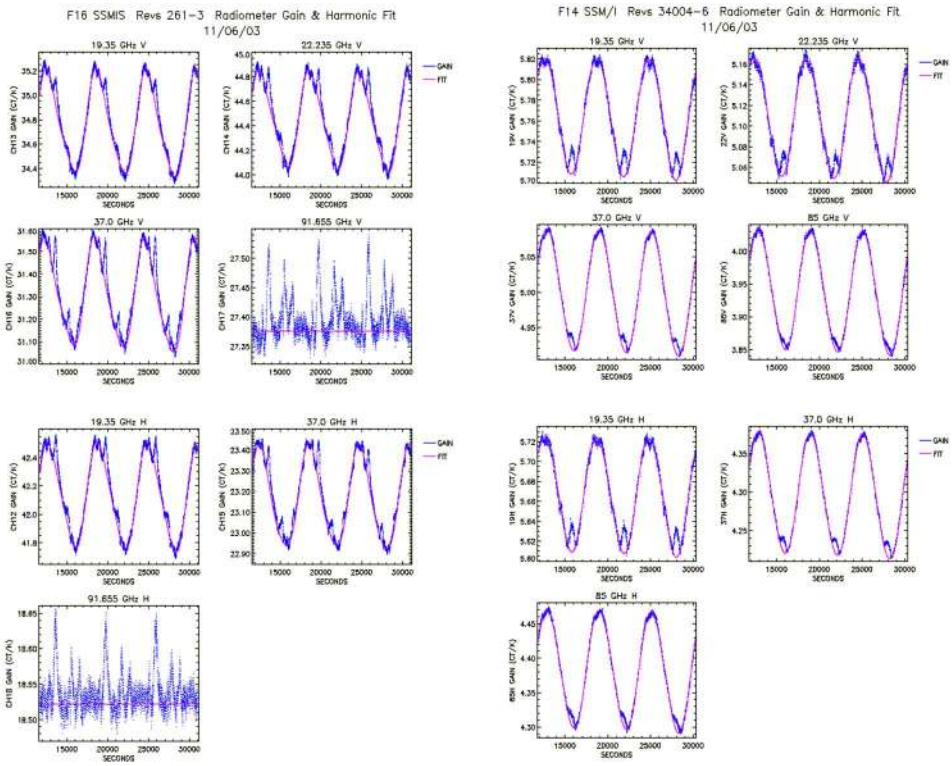

Fig. 12. SSMIS (a) SSM/I (b) radiometer gain (blue) without and (red) with correction for solar intrusions into the warm load November 6, 2003. Local gain peaks are removed in the red functions.

facilitated by the Channel 17 and Channel 18 radiometer gains that are very stable due to the local proportional (pulsewidth modulated) heater that keeps their receiver temperatures a factor of ∼10 more stable compared to others on SSMIS. Similar investigations involving calibration of DMSP F-14 SSM/I data revealed solar intrusions into the SSM/I warm load, primarily over both poles [Fig. 12(b)] that were previously unknown.

F. Reflector Emission

Another method of evaluating SSMIS SDR calibration accuracy and stability involved comparisons with global analysis fields from the ECMWF NWP model applied to the RTTOVS-7 forward radiative transfer model (RTM) to simulate SSMIS observations. Channels within the SSMIS lower atmospheric temperature sounding suite that do not contain significant contributions from surface emission show a smooth slowly varying background over which sensor calibration anomalies are readily apparent by examination. Accordingly, for Channels 3, 4, and 5, residual biases were observed to be on the order of ∼2–3 K (Fig. 13). Larger biases were observed in Channels 9–11 (183.31 GHz), although, the exact nature of the residual was difficult to determine due to atmospheric variability present in these channels that are sensitive to atmosphere moisture.

The cause of the residual bias described above was attributed to emission from the SSMIS main reflector after the detailed development of an SSMIS simulation tool confirmed that sun-illumination of the SSMIS main reflector surface was highly correlated with changes in the bias [6], [7], and [11]. Systematic seasonal biases observed with upward looking LIDAR measurements carried out at Barking Sands in Hawaii also supported the conclusion of emission from the SSMIS main reflector as the source of the recurring bias found in the SSMIS ascending phase [12]. For F-16, the residual bias changes most dramatically over the course of several scans typically in the region ∼0° to 70° N latitude depending on the orbital season. Reflector emission was not addressed in the EDR analysis and SDR comparisons with F-14.

V. EDR Performance Analysis

A. Surface and SSM/I Heritage EDRS

Overall, the SSMIS EDR performance was evaluated using four approaches: 1) the F-14 cross-validation performance; 2) shipboard measurements; 3) the FNMOC buoy wind speed measurements; and 4) the FNMOC island RAOB matchups. Detailed intersensor comparisons with F-14 using the three data sets described in the previous section were performed for several EDRs: Wind Speed, Water Vapor, Land Surface Type, Land Surface Temperature, Sea Ice Concentration, Ice Edge, Rain, and Hurricane Imagery. The EDR comparisons were performed in a similar manner as the SDR intercomparisons, showing that F-16 SSMIS achieves similar heritage EDR performance as F-14 with SSM/I on a global average basis.

The SSMIS imaging EDR algorithms are those currently used operationally by SSM/I ground data processing as defined in the SSM/I Algorithm Specification Document [13]. Many of the heritage algorithms come directly from the earlier SSM/I

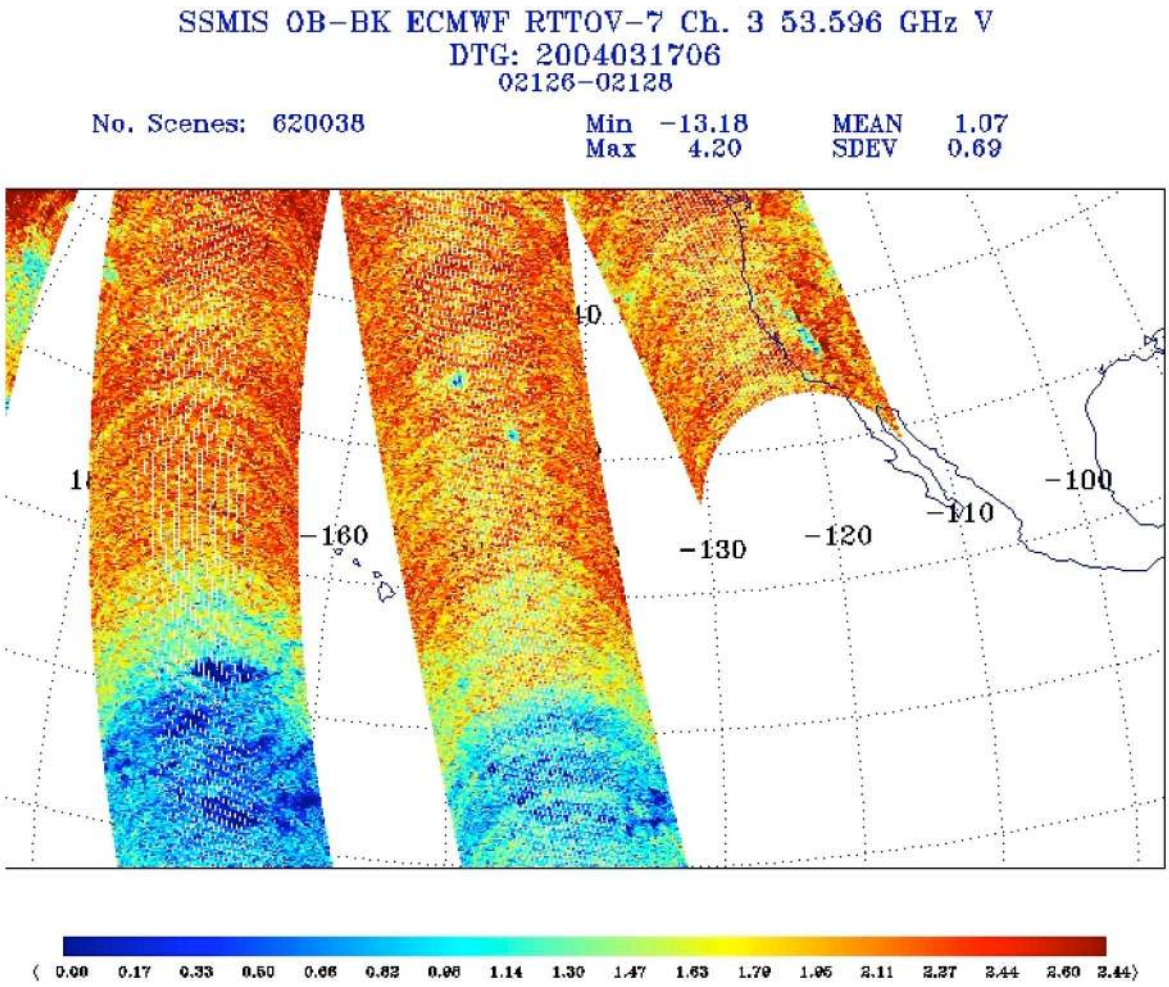

Fig. 13. ECMWF analysis fields subtracted from SSMIS observations for Channel 13 on March 17, 2004 for the ascending phase showing the impact of increased reflector emission due to heating of the main reflector from solar illumination.

as reported in the DMSP SSM/I cal/val report [14], [15]. The algorithms use brightness temperatures from Channels 12–18 to compute the surface and heritage EDRs [16]. An initial performance estimate of F-16 SSMIS-derived precipitable water and ocean surface wind speed are provided below [17], [18].

Comparisons of SSMIS measurements were made with upward-looking radiometer measurements conducted aboard the RV Brown from October 15 to November 20, 2003 in the location of 8° S to 12° N latitude and between 85° and 110° W longitude. In these comparisons, differences between precipitable water measured by SSMIS and NOAA/ETL indicated that the SSMIS data demonstrated good correlation but were biased slightly high $(\mu = 1.40; \sigma = 2.30)$ in millimeters, over the range of ∼25–60 mm.

Comparisons of SSMIS-measured wind speed with FNMOC's globally distributed buoy database were collected using space and time coincidence windows of 25 km and 30 min, respectively. The comparisons indicated that performance of F-13, F-14, and F-15 SSM/I and F-16 SSMIS data were very similar for the period between November 2003 and July 2005 (Fig. 14). The number of observations N was $> 20\,000$ for all sensors with the mean difference $\mu < 0.2$ m/s for all cases and σ between 1.7 and 1.9 m/s. Similarly, for integrated water vapor comparisons with the FNMOC ISIS island RAOB database, N was ∼2000 or greater for all sensors with the mean difference μ between 1.4 and 1.9 mm, and the standard deviation σ between 3.5 and 3.7 mm, as shown in Fig. 15.

Overall, the SSM/I heritage EDR algorithms performed as expected on a global statistical basis with occasional small regional biases due to 1) imperfect corrections for calibration errors due to sun intrusion into the warm load and 2) reflector antenna emission during entry and exit of Earth shadow. For example, the ocean wind speed and land surface temperature EDRs exhibited regional biases on the order of 0.5–1 m/s and 1–1.5 K, respectively.

B. Temperature Sounding EDRs

During the cal/val, SSMIS lower atmospheric sounding (LAS) validation efforts were applied to data collected between November 2003 and December 2004. The complete LAS study is based on matchup comparisons between collocated SSMIS EDRs and observations by operational radiosondes, ECMWF analysis fields, and data from the Barking Sands LIDAR campaign [12]. The atmospheric temperature EDR algorithm

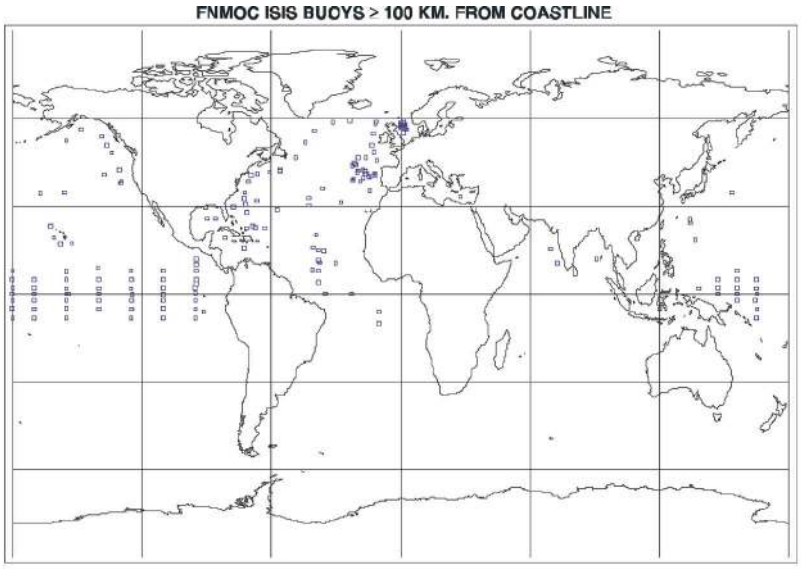

(a)

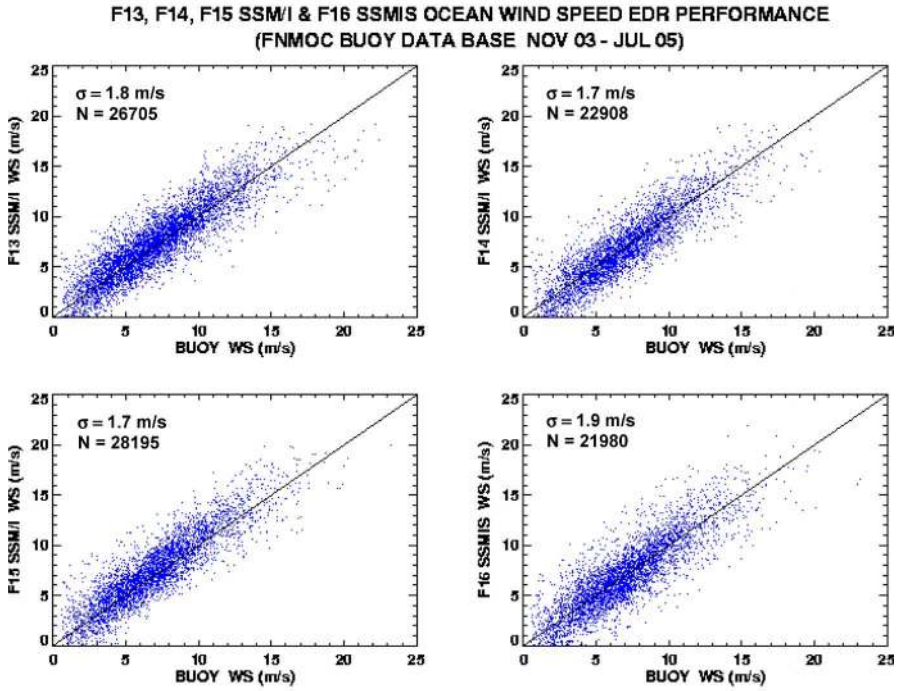

(b)

Fig. 14. (a) FNMOC ISIS database ocean buoy locations and (b) DMSP F-13, F-14, and F-15 SSM/I, and F-16 SSMIS ocean wind speed performance with mean differences $\mu < 0.2$ m/s (FNMOC buoy database November 2003–July 2005).

is a stratified regression algorithm based on air mass characteristics that provides a separate retrieval for each of three atmosphere types: 1) high tropopause $P'_{\mathrm{Trop}} < 120$ mb; 2) medium altitude tropopause $120 < P'_{\mathrm{Trop}} < 250$ mb; and 3) low tropopause $P'_{\mathrm{Trop}} > 250$ mb [16]. Unfortunately, the selection process involves Channel 1 that was determined to have the incorrect polarization (V-pol instead of H-pol) for the F-16 SSMIS. This error significantly impacts the LAS EDR performance.

As a result of incorrect polarization and additional required changes, the GDPS was updated (Revision 5) during the cal/val to alter the LAS algorithm to best account for the polarization error in Channels 1–5, improve the geolocation, and correct for edge-of-scan effects. However, changes to the LAS algorithm to account for polarization were found to only provide a small improvement in LAS performance, preventing a full evaluation of the SSMIS LAS capability. Because of this result, all remaining SSMIS sensors were changed to incorporate H-pol in Channels 1–5 as originally designed.

In Fig. 16, SSMIS LAS retrievals are compared to ECMWF analysis fields using spatially collocated matchups that are time interpolated between the nearest 6-h runs for all three atmosphere types. The 90% statistical confidence uncertainty value shown in light gray (blue) for each level. The bias, shown

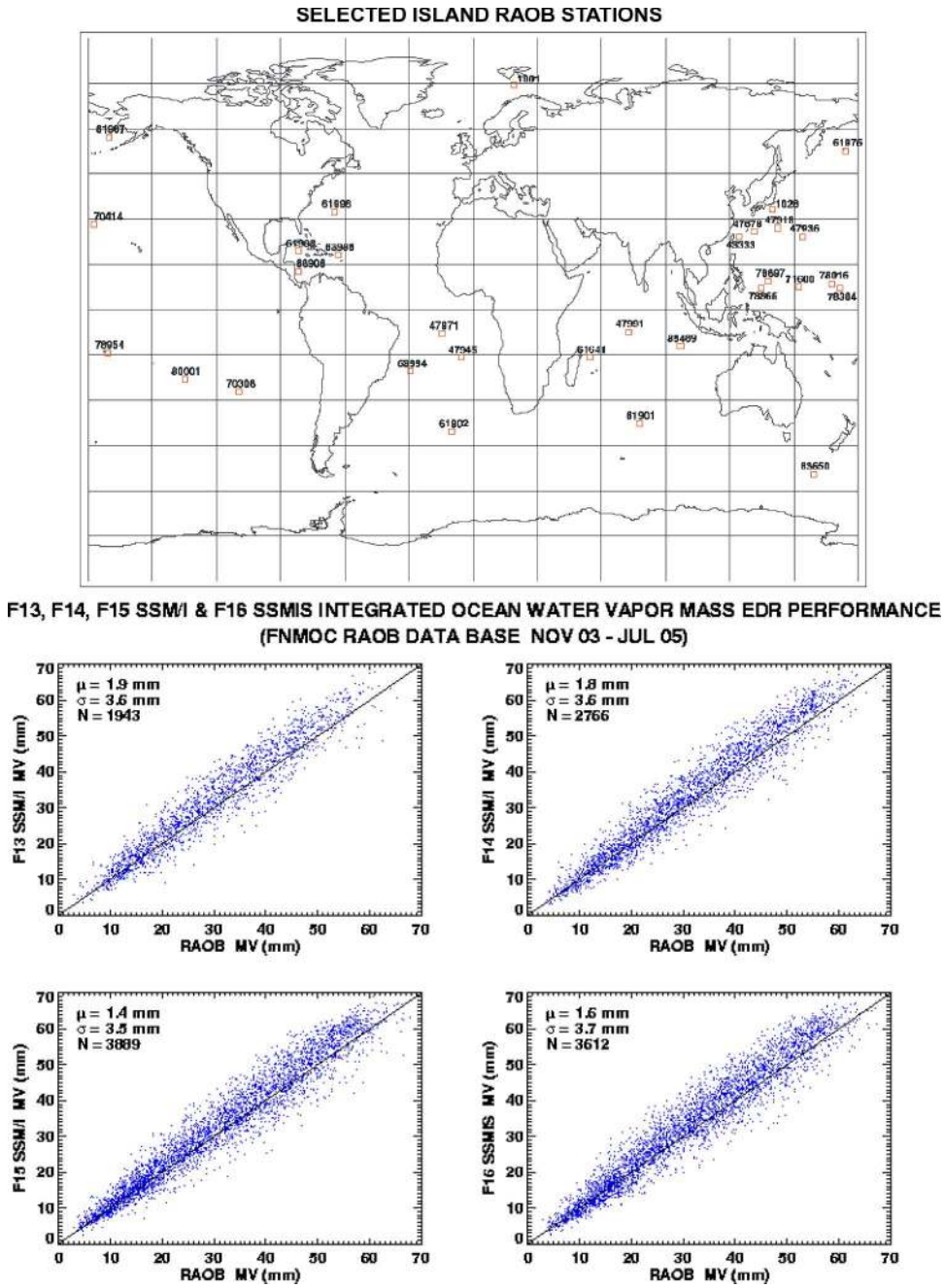

Fig. 15. (a) FNMOC ISIS island RAOB database. (b) DMSP F-13, F-14, F-15 SSM/I, and F-16 SSMIS integrated water vapor mass EDR performance (FNMOC RAOB database November 2003–July 2005).

in dark gray (red), and rms error in white (yellow) exceed specification (dashed line) for several atmospheric levels within each atmosphere type. Much of the excess rms and bias error is attributed to incorrect polarization of the LAS channels that inhibits the LAS algorithm from correctly preclassifying the atmosphere (even after attempting to mitigate this problem in version 5 of the GDPS). The positive overall bias may also be partially attributed to the reflector calibration anomaly (see Fig. 13). Similar results are found with RAOB and LIDAR matchups [12]. Although the SSMIS EDR specification is not explicitly met using the supplied LAS algorithm, studies involving SSMIS sounding SDR data applied to NWP models have shown the value of SSMIS and Advanced Microwave Sounding Unit (AMSU) data to be similar if SSMIS data impacted by the calibration anomalies are removed [19].

C. UAS

The SSMIS UAS channels represent a unique capability to monitor the atmospheric state at altitudes well into the mesosphere (∼0.01 mb). This is achieved by radiometers utilizing analog passbands with multiple ∼0.002% bandwidths, frequency stability to within ∼1 ppm, and Doppler compensation for the conical scan geometry to a frequency scale well below that. The SSMIS UAS channels are an engineering achievement for space-based radiometry.

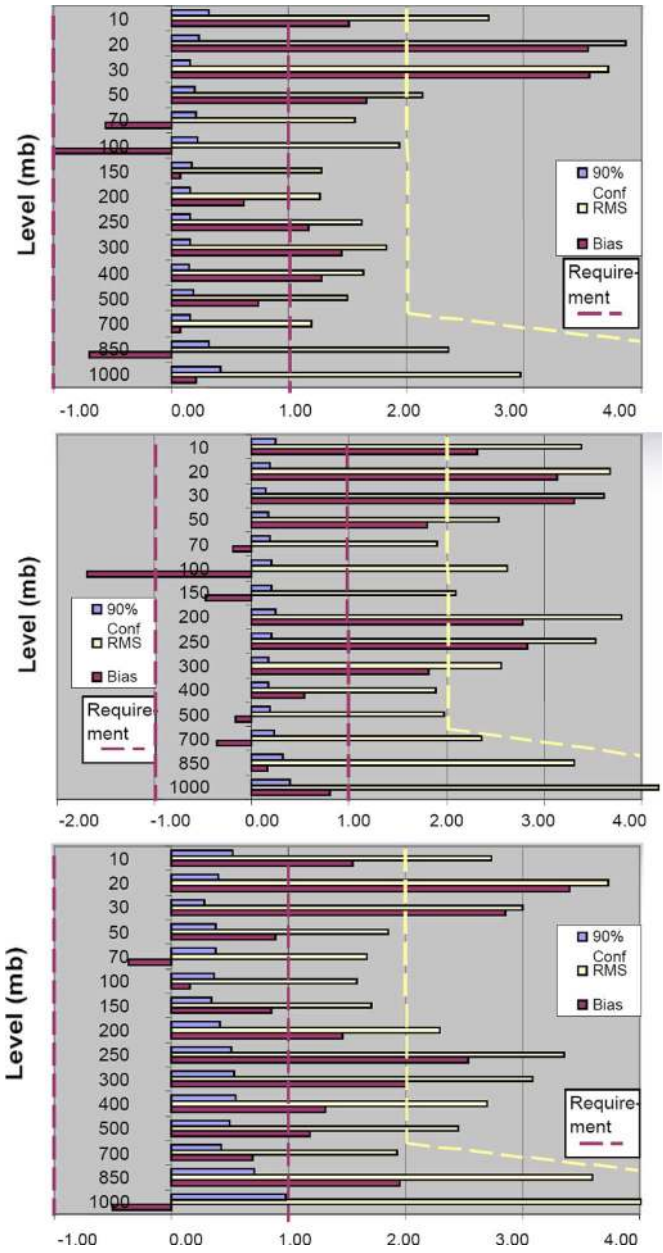

Fig. 16. Lower atmospheric temperature EDR versus ECMWF for winter 2003 using GDPS Revision 5 corrections. (a) $P'_{\mathrm{Trop}} < 120$ mb. (b) $120 < P'_{\mathrm{Trop}} < 250$ mb. (c) $P'_{\mathrm{Trop}} > 250$ mb.

There are three main objectives of the SSMIS UAS cal/val effort: 1) verify end-to-end instrument radiometric calibration accuracy accounting for Doppler compensation; 2) verify the calibration of the UAS SDRs; and 3) validate the UAS temperature retrievals using independent measurements of temperature profiles. To help achieve these objectives, a LIDAR campaign to produce high-quality temperature profiles was planned to be the primary data source for SDR calibration and EDR validation. In addition, ECMWF NWP analyses were used for broad geographic validation of EDRs from 7–0.1 hPa (7–0.1 mb). Details of the UAS cal/val effort can be found in [20], and additional background on mesospheric measurements in [21]. An example of the UAS Channel 19 SDRs shows the effect of Doppler frequency during the scan [Fig. 17(a)], with systematic warmer temperatures appearing at the center of the sensor swath. This is due to the effective height of the temperature weighting function decreasing, moving to a lower warmer level of the mesosphere near the center of scan, because the apparent frequency of the scene is higher at the center of scan when the SSMIS is observing in the direction of the spacecraft velocity. The UAS brightness temperatures, and hence, the inversion algorithm are also dependent on the Earth's magnetic field [22].

When the SSMIS is operating with Doppler compensation enabled, the center frequency of each sounding channel is scanned to precisely track frequency shifts of the scene caused by the conical scan geometry and spacecraft motion. The result [Fig. 17(b)] shows that the weighting function is stable across the swath as suggested by the slowly varying random characteristics of the SDR image, confirming proper operation of the UAS narrowband radiometers.

VI. Numerical Weather Prediction

The NWP models have played an important role in the SSMIS cal/val. First, the NWP analysis fields when combined with suitable radiative transfer models (containing SSMIS channel spectral pass-bands and scan geometry) provide synoptic-scale simulated brightness temperature imagery that may be differenced with coincident SSMIS imagery to verify orbital instrument calibration stability as well as detection of anomalous instrument behavior. Second, after removal of instrument scan bias and radiative transfer model errors NWP data assimilation experiments may be conducted to assess the benefits of SSMIS observations in improving NWP forecast quality.

For lower atmospheric temperature sounding channels, the uncertainty in NWP analyses, or short-range forecast fields (at $T + 6$ h, also known as *background* fields), is estimated to be in the range of 0.2–0.4 K. This high level of accuracy has facilitated the detection of the two major anomalies which adversely affect the SSMIS LAS channels. The magnitude of these effects ($\sim$1–1.5 K) has made the detailed study of their orbital and seasonal behavior possible using global NWP data, and this work is described both within and outside this issue [7], [19], [23], and [24]. Based on these studies, physically based corrections and averaging schemes have been developed which have improved the quality of SSMIS LAS brightness temperatures by factors of 3–4. Observed minus background departures for tropospheric temperature sounding channels have been reduced from initial values of 1.0–1.5 K to approximately 0.3–0.4 K (at 1 standard deviation). Further improvements are anticipated as correction strategies are refined. The NWP fields have also been important in the validation of brightness temperatures from the SSMIS imaging and environmental channels. Although, due to higher uncertainties in modeling surface effects and in modeling global water vapor fields, uncertainties in the modeled brightness temperature are also larger for these channels, typically 2–4 K. This approach complements that described in this issue in which collocated radiosonde profiles mapped into top-of-atmosphere brightness temperatures provide the independent validating data source [12].

The direct assimilation of radiances is an important means of exploiting passive microwave observations from satellites

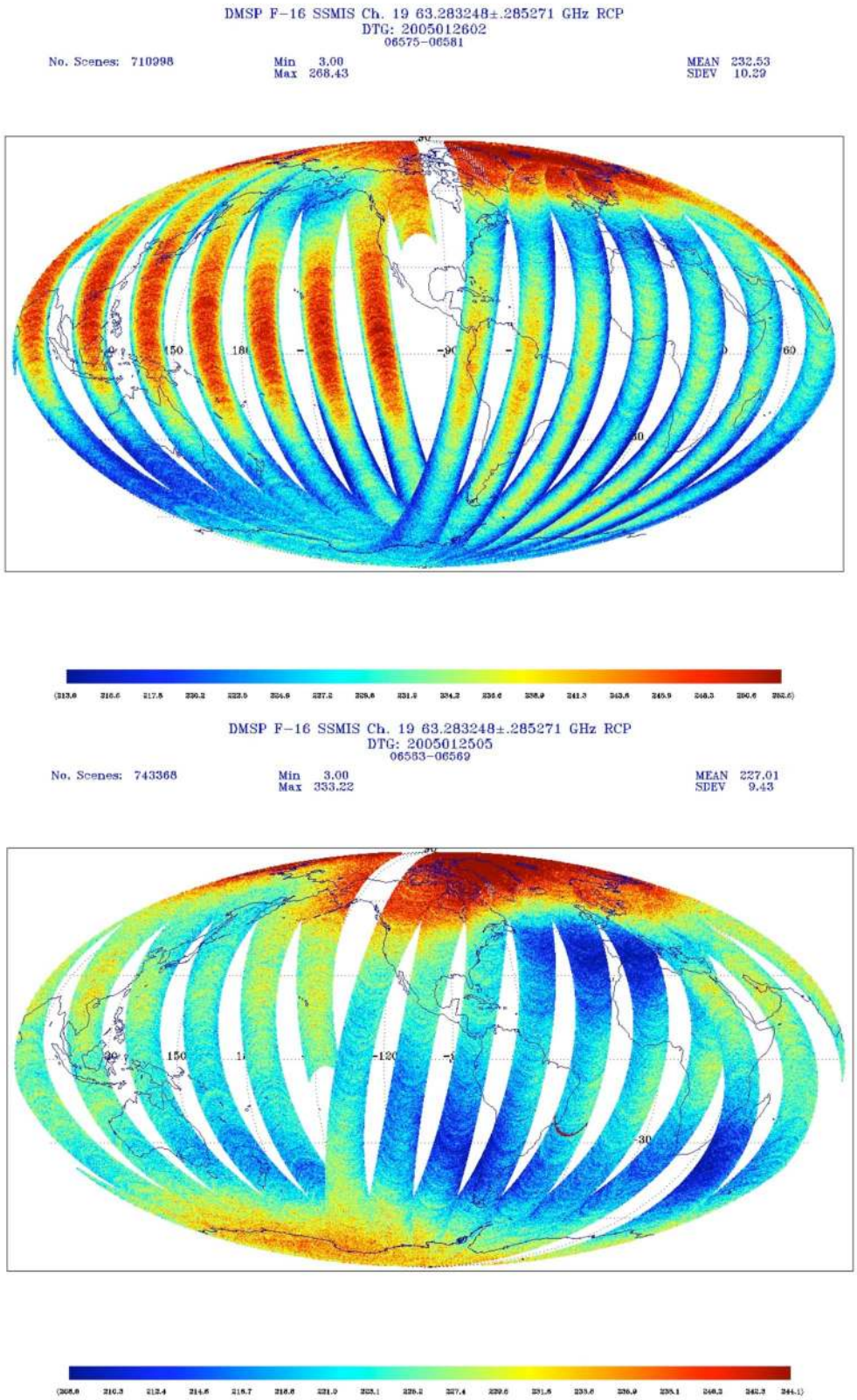

Fig. 17. DMSP F-16 SSMIS Channel 19 SDRs from January 25 and 26, 2005. (a) SSMIS operating in the "Doppler off" mode where SDRs show scan-position-dependent temperatures due to changes in the effective height of the temperature weighting functions over the scan. (b) SSMIS operating in the "Doppler on" mode showing the scan position dependence of brightness temperatures largely removed.

at most NWP centers, and microwave sounding and imaging data have become very important in maintaining and improving forecast quality in both hemispheres. A high-priority requirement for this large and growing user group is high-quality brightness temperature observations. The requirements are particularly stringent for the lower atmospheric temperature

sounding channels, where high-quality background fields demand equally high-quality radiances (with uncertainties in the range 0.1–0.3 K) to improve analyses and, hence, forecast accuracy.

Assimilation experiments have been carried out at four NWP centers (NCEP, NRL, ECMWF, and the Met Office, UK) using corrected SSMIS brightness temperatures [19]. Most of these studies have focused on the use of lower atmospheric temperature sounding data. Significantly, these studies have shown that in baseline experiments in which no other satellite sounding data are used in the assimilation, SSMIS temperature sounding channels deliver $\sim$67% of the impact (in terms of improvement in forecast quality) of a single AMSU. This result is encouraging given the residual biases still evident in the corrected SSMIS data and the potential for further improvement in F-16 corrections and through hardware modifications to future sensors (F-17–F-20). In experiments in which SSMIS data are added to full operational assimilation systems, the impact is mainly neutral-positive in the Southern Hemisphere with PMSL Day 1–4 forecast errors reduced by 0.5%–2.5%. Assimilation experiments have also shown the value of SSMIS data in improving the representation and forecasting of tropical storms [25], [26].

Further benefits for the NWP community are expected from the exploitation of temperature sounding channels which peak near the surface [27], from the exploitation of the SSMI-like channels [28] and from the UAS channels now that fast RT models [29] dealing with Zeeman splitting are available. As the model lid at many operational NWP centers is raised, SSMIS offers the only operational sensor able to provide temperature information in the altitude range of 40–80 km.

VII. Summary

In this paper, an overview was provided of the instrument design and characteristics of the first SSMIS along with major cal/val results. The SSMIS instrument was found to exhibit remarkably stable radiometer sensitivities, meeting requirements with considerable margin, while providing high-quality imagery for all channels. Time and angular misalignment offsets were developed and incorporated in the GDPS, resulting in geolocation accuracy that was both stable and meeting requirements with typically lower than 4–5 km errors. Corrections were developed and implemented in the GDPS to remove along-scan biases at the start-of-scan and end-of-scan regions, thereby preserving the 1700-km swath width. Aircraft underflights of the SSMIS by APMIR and CoSMIR assisted in the determination of absolute calibration accuracy and stability as well as confirming that the polarizations of Channels 1–5 were inadvertently vertically polarized rather than the desired horizontal polarization. Subsequent SSMIS instruments have been modified to make these channels horizontally-polarized. Coincidence of satellite orbits permitted intersensor comparisons and cross calibration between the SSMIS with corresponding F-14 SSM/I channel SDRs. Statistical results show the SSMIS SDRs may be mapped with appropriate slopes and offsets into SSM/I SDRs to obtain comparable performance of SSMI-type EDRs for all surface types.

Two important calibration anomalies were uncovered during the cal/val program: 1) periodic solar heating of the tip of the tines of the warm-load calibration target and 2) relatively large main reflector microwave emission, most notable when the antenna entered/exited Earth shadow. As part of the cal/val, a number of sophisticated analysis and simulation tools were developed to understand and characterize the source of the anomalies and found to be very valuable in the design and development of hardware modifications to mitigate the anomalies in future SSMIS instruments. Background NWP analysis fields have played a central role in these efforts.

Significant cal/val resources were dedicated to obtain high-quality validation data for the sounding and imaging EDRs. These include special LIDAR observations by Jet Propulsion Laboratory (JPL), University of Alaska, and The Aerospace Corporation, aircraft dropsonde campaigns by NOAA AOC, shipboard measurements by NOAA ETL, global operational radiosonde observations, NWP analysis and forecast fields, auxiliary satellite sensor data, and special asynoptic radiosonde observations. Although hampered by the calibration anomalies noted above, the EDR validation effort provided valuable insights into the relative contributions of all error sources, the major issues and limitations associated with the process of validating satellite EDR sounding products, the strengths and weaknesses of SSMIS conical sounding capability, and a performance assessment of regression-based sounding algorithms.

Finally, we have found that the shift toward radiance assimilation has necessitated a change in emphasis from the validation of EDRs to the validation of measured brightness temperatures. Indeed, the majority of analysis effort during the SSMIS cal/val was directed at characterizing and improving SDR quality. This perspective is expected to become more even important for future operational sensors to meet the needs of the large and growing section of the user community engaged in direct radiance assimilation.

Appendix

After submission of this paper, the DMSP cal/val team of the second SSMIS instrument (F-17) found anomalous reflector emissions exist in the scene observations comparable to those found in F-16 SSMIS data. Recent laboratory measurements and analysis of other SSMIS flight-unit reflectors suggest that F-16 and F-17 SSMIS reflectors have extremely low surface electrical conductivities that perhaps arise from excessive surface roughness and insufficient VDA thickness. As part of the cal/val team's recommendation, procedures to measure the conductivity and emissivity of the main reflector antennas are now in place for future SSMIS instruments. The main reflector of the third SSMIS instrument (F-18) scheduled for launch in mid-2008 was found to have poor conductivity and has been replaced with a spare reflector having significantly higher conductivity (17–18.5 MS/m) that will hopefully reduce the on-orbit F-18 reflector emission to a negligible level.

Acknowledgment

The authors would like to thank Col. Wagner, Director of DMSP and Mr. T. Piwowar (Navy, PMW-180) for their

strong support and encouragement in the performance of the SSMIS cal/val program; Air Force Col. R. Odle (former Director of DMSP), Ms. Smith (Deputy Director), Mr. Weeks (former Deputy Director), and Capt. Chambers (DMSP SSMIS Program Manager) for their enthusiasm and support; Cdr. Gottshall, Mr. Godin, and Mr. Berkowitz (PMW-180) for their strong and steady support; Mr. B. Thomas, Dr. A. Fote, and Ms. A. Kishi (Aerospace), and Dr. Tesmer of FNMOC for providing SSMIS data products and supporting cal/val data; Dr. M. Werner and Dr. M. Meshishnek (Aerospace) for their support; and Dr. Shapiro (UCAR), Dr. Parrish (NOAA AOC), Dr. McDermid (JPL), Prof. Collins (U. Alaska), Dr. Hazen, Dr. Post, Dr. Westwater, Dr. Fairall, and Dr. Wolf (NOAA ETL), and Dr. Bougeault, Dr. Hollingsworth, Dr. McNally, Dr. Kelly, Dr. Hennessey, and Dr. Burridge (ECMWF) and ECMWF operations for providing exceptionally high-quality validation data without which this cal/val effort would have been severely limited.

REFERENCES

[1] J. P. Hollinger, J. L. Peirce, and G. A. Poe, "SSM/I instrument evaluation," *IEEE Trans. Geosci. Remote Sens.*, vol. 28, no. 5, pp. 781–790, Sep. 1990.

[2] G. Poe, K. St. Germain, J. Bobak, S. Swadley, J. Wessel, B. Thomas, J. Wang, and B. Burns, "DMSP calibration/validation plan for the Special Sensor Microwave Imager Sounder (SSMIS)," Naval Research Laboratory, Oct. 2001.

[3] F. T. Ulaby, R. K. Moore, and A. K. Fung, *Microwave Remote Sensing, Active and Passive*, vol. 1. Norwood, MA: Artech House, 1981.

[4] G. A. Poe, E. A. Uliana, B. A. Gardiner, T. E. vonRentzell, and D. B. Kunkee, "Geolocation error anaysis of the Special Sensor Microwave Imager/Sounder," *IEEE Trans. Geosci. Remote Sens.*, vol. 46, no. 4, pp. 913–922, Apr. 2008.

[5] D. B. Kunkee, Y. Hong, D. A. Thompson, M. F. Werner, and G. A. Poe, "Analysis of the Special Sensor Microwave Imager/Sounder (SSMIS) fields of view on DMSP F-16," *IEEE Trans. Geosci. Remote Sens.*, vol. 46, no. 4, pp. 934–945, Apr. 2008.

[6] D. B. Kunkee, S. D. Swadley, G. A. Poe, Y. Hong, and M. F. Werner, "Special Sensor Microwave Imager Sounder (SSMIS) radiometric calibration anomalies—Part I: Identification and characterization," *IEEE Trans. Geosci. Remote Sens.*, vol. 46, no. 4, pp. 1017–1033, Apr. 2008.

[7] S. D. Swadley, G. A. Poe, D. B. Kunkee, Y. Hong, and M. F. Werner, "Special Sensor Microwave Imager Sounder (SSMIS) radiometric calibration anomalies—Part II," *IEEE Trans. Geosci. Remote Sens.*, submitted for publication.

[8] J. R. Wang, P. E. Racette, and J. R. Piepmeier, "A comparison of near concurrent measurements from SSMIS and CoSMIR for some selected channels over the frequency range of 50–183 GHz," *IEEE Trans. Geosci. Remote Sens.*, vol. 46, no. 4, pp. 923–933, Apr. 2008.

[9] J. P. Bobak, D. J. Dowgiallo, T. E. vonRentzell, and N. R. McGlothlin, "Satellite calibration and validation utilizing the Airborne Polarimetric Microwave Imaging Radiometer (APMIR)," in *Proc. MTS/IEEE Oceans*, Sep. 2005, vol. 1, pp. 352–354.

[10] J. P. Bobak, D. J. Dowgiallo, N. R. McGlothlin, and T. E. vonRentzell, "Calibration and validation activities of the Airborne Polarimetric Microwave Imaging Radiometer—APMIR," in *Proc. IGARSS*, Sep. 2004, vol. 5, pp. 3286–3287.

[11] D. B. Kunkee, D. J. Boucher, G. A. Poe, and S. Swadley, "Evaluation of the Defense Meteorological Satellite Program (DMSP) Special Sensor Microwave Imager Sounder (SSMIS)," in *Proc. Int. Geosci. Remote Sens. Symp.*, Denver, CO, Jul. 2006, pp. 101–104.

[12] J. Wessel, R. W. Farley, A. Fote, Y. Hong, G. A. Poe, S. D. Swadley, B. Thomas, and D. J. Boucher, "Calibration and validation of DMSP SSMIS lower atmospheric sounding channels," *IEEE Trans. Geosci. Remote Sens.*, vol. 46, no. 4, pp. 946–961, Apr. 2008.

[13] "Raytheon Technical Report," USAF Space and Missile Systems Center. AS 32268-100, Contract F04701-96-C-0026, DMSP, 1996.

[14] J. P. Hollinger, "DMSP Special Sensor Microwave/Imager calibration/validation," Naval Res. Lab., Washington, DC, Jul. 1989. Final Report.

[15] J. P. Hollinger, "DMSP Special Sensor Microwave/Imager calibration/validation," Naval Res. Lab., Washington, DC, Jul. 1991. Final Report.

[16] *Algorithm and Data User Manual (ADUM) for the SSMIS*, Jul. 2002, Azusa, CA: Northrop Grumman Corp., Electron. Syst. Division. Contract F04701-00-C-0001.

[17] J. C. Alishouse, S. A. Synder, J. Vongsathorn, and R. A. Ferraro, "Determination of oceanic total precipitable water from the SSM/I," *IEEE Trans. Geosci. Remote Sens.*, vol. 28, no. 5, pp. 811–816, Sep. 1990.

[18] M. A. Goodberlet, C. T. Swift, and J. C. Wilkerson, "Ocean surface wind speed measurements of the Special Sensor Microwave/Imager (SSM/I)," *IEEE Trans. Geosci. Remote Sens.*, vol. 28, no. 5, pp. 823–827, Sep. 1990.

[19] W. Bell, S. J. English, B. Candy, N. Atkinson, F. Hilton, N. Baker, S. D. Swadley, W. F. Campbell, N. Bormann, G. Kelly, and M. Kazumori, "The assimilation of SSMIS radiances in numerical weather prediction models," *IEEE Trans. Geosci. Remote Sens.*, vol. 46, no. 4, pp. 884–900, Apr. 2008.

[20] S. D. Swadley, G. A. Poe, W. Bell, Y. Hong, D. B. Kunkee, I. S. McDermid, and T. Leblanc, "Analysis and characterization of the SSMIS upper atmospheric sounding channel measurements," *IEEE Trans. Geosci. Remote Sens.*, vol. 46, no. 4, pp. 962–983, Apr. 2008.

[21] A. Stogryn, "Mesospheric temperature sounding with microwave radiometers," *IEEE Trans. Geosci. Remote Sens.*, vol. 27, no. 3, pp. 332–338, May 1989.

[22] A. Stogryn, "The magnetic field dependence of brightness temperatures at frequencies near the O_2 microwave absorption lines," *IEEE Trans. Geosci. Remote Sens.*, vol. 27, no. 3, pp. 279–289, May 1989.

[23] D. X. Kerola, "Calibration of Special Sensor Microwave Imager/Sounder (SSMIS) upper air brightness temperature measurements using a comprehensive radiative transfer model," *Radio Sci.*, vol. 41, RS4001, 2005. DOI:10.1029/2005RS003329.

[24] B. Yan and F. Weng, "Intercalibration Between Special Sensor Microwave Imager/Sounder and Special Sensor Microwave Imager," *IEEE Trans. Geosci. Remote Sens.*, vol. 46, no. 4, pp. 984–995, Apr. 2008.

[25] Q. Liu and F. Weng, "Radiance assimilation in studying Hurricane Katrina," *Geophys. Res. Lett.*, vol. 33, no. 22, L22811, 2006.

[26] Q. Liu and F. Weng, "Detecting the warm core of a hurricane from the Special Sensor Microwave Imager Sounder," *Geophys. Res. Lett.*, vol. 33, no. 6, L06817, 2006.

[27] F. Karbou, N. Bormann, and J.-N. Thépaut, "Towards the assimilation of satellite microwave observations over land: Feasibility studies using SSMI/S, AMSU-A and AMSU-B," Eumetsat Satellite Application Facility for Numerical Weather Prediction (NWPSAF) Rep. NWPSAF-EC-TR-000, Jan. 2006.

[28] N. Bormann, G. Kelly, P. Bauer, and W. Bell, "Assimilation and monitoring of SSMIS, AMSR-E and TMI data at ECMWF," in *Proc. Int. TOVS Study Conf.*, Maratea, Italy, 2006.

[29] Y. Han and F. Weng, "A fast radiative transfer model for SSMIS upper air sounding channels affected by Zeeman splitting: Application for temperature retrieval," in *Proc. Int. TOVS Study Conf.*, Maratea, Italy, 2006.

David B. Kunkee (S'88–M'96–SM'04) received the Ph.D. degree in electrical engineering from the Georgia Institute of Technology, Atlanta, in 1995.

He joined The Aerospace Corporation, Los Angeles, CA, in 1995 and is currently an Associate Director. He is a Technical Advisor and a Sensor Scientist with the National Polar-orbiting Operational Environmental Satellite System (NPOESS) integrated program office involved with the development and planning for the new NPOESS Microwave Imager/Sounder. He is also a core member of the Defense Meteorological Satellite Program's Special Sensor Microwave Imager/Sounder Calibration/Validation team.

Dr. Kunkee is a member of the International Union of Radio Science, URSI (Commission F) and has served on the National Academies' Committee on Radio Frequencies. He is currently Editor of the IEEE GEOSCIENCE AND REMOTE SENSING SOCIETY (GRS-S) NEWSLETTER and the past Chair of the GRS-S Technical Committee on Frequency Allocations in Remote Sensing.

Gene A. Poe (M'91) received the B.A. and M.S. degrees in electrical engineering from the University of California, Berkeley, in 1964 and 1965, respectively.

He has worked in wide-ranging capacities for major aerospace companies responsible for the development of space-based passive microwave instruments (Aerojet Corporation, Sacramento, CA, 1965–1972 and 1989–1993; Hughes Aircraft Company, Culver City, CA, 1976–1982). His experiences in microwave radiometry include analyzing laboratory and field measurements, development of emissivity models, and participating in the design of space sensors (DMSP SSM/I, SSMIS, SSM/T-2, and NOAA AMSU). From 1986 to 1989, he was with the Space Sensing Branch, Naval Research Laboratory, Washington, DC, on passive microwave modeling and analysis of SSM/I data. In 1993, he rejoined the Naval Research Laboratory to lead the Calibration/Validation program for the SSMIS instrument and is currently with the Satellite Meteorology Branch, Monterey, CA.

Donald J. Boucher received the B.A and M.S. degrees in meteorology from the University of California, Los Angeles.

He joined the Space Sciences Laboratory, Aerospace Corporation, Los Angeles, in 1976. His early work concentrated on atmospheric numerical modeling. In 1983, he moved to the DMSP program office to head the development of the Satellite Data Handling System for the Air Force Weather Agency. He has headed the instrument and algorithm efforts for DMSP and has recently completed successful Calibration/Validation's for the Special Sensor Microwave Imager Sounder on DMSP Flight's 16 and 17. He is currently a Principal Engineer with the Space Support Division.

Steven D. Swadley (M'00) received the B.S. and M.S. degrees in meteorology from San Jose State University, San Jose, CA, in 1981 and 1983, respectively, and the M.S. degree in applied mathematics from the US Naval Postgraduate School, Monterey, CA, in 1988.

He is currently the proprietor of METOC Consulting, Monterey, specializing in satellite meteorology and atmospheric data assimilation systems. He is currently supporting the data assimilation and satellite applications sections of the Naval Research Laboratory Marine Meteorology Division, Monterey. He has worked extensively with microwave radiance assimilation systems and is a core member of the SSMIS Cal/Val teams for F-16 and F-17.

Ye Hong received the B.S. degree in electrical engineering from Zhejiang University, Hangzhou, China, the M.S. degree in electrical engineering from the Chinese Academia of Sciences, Beijing, and the Ph.D. degree in satellite meteorology from Texas A&M University, College Station.

She is currently with The Aerospace Corporation, Los Angeles, CA, working on the Defense Meteorological Satellite Program SSMIS Cal/Val and supporting the NPOESS MIS algorithm development. Prior to joining Aerospace, she was a Research Scientist and worked on precipitation algorithm development and data analysis for the NASA TRMM project, as well as the TRMM Science Data and Information System.

John E. Wessel received the B.S. degree in chemistry from the University of California, Los Angeles, in 1965 and the Ph.D. degree in chemical physics from the University of Chicago, Chicago, IL, in 1970.

From 1970–1974, he was a Postdoctoral Fellow and Instructor of Chemistry at the University of Pennsylvania, where he conducted research in the area of laser spectroscopy. He joined The Aerospace Corporation, El Segundo, CA, in 1974 and has conducted research in molecular, atomic, semiconductor, and surface spectroscopies. He served as Principal Investigator in programs sponsored by the National Science Foundation, the Air Force Office of Scientific Research, the Department of Energy, and The Aerospace Corporation. He retired as a Distinguished Scientist and continues working part time in the Photonics Technology Department at Aerospace, involved in meteorological lidar and satellite remote sensing programs.

Dr. Wessel is a member of the American Physical Society, American Chemical Society, American Association for the Advancement of Science, and Sigma Xi.

Enzo A. Uliana received the B.S. degree in mathematics from St. Mary's University, San Antonio, TX, in 1958.

Since 1959, he has been with the Naval Research Laboratory, Washington, DC, both as an employee (1959–1997) and a contractor (1997–present) in various fields ranging from the analysis of underwater acoustic data to space-based radar system data. He was involved in the analysis of radar altimeter data from Skylab through Topex. Since 1993, he has been involved with the calibration and validation of the SSM/I and SSMIS passive microwave data systems. He has developed many tools to simplify the analysis of the data. He is currently with Interferometrics, Inc., Herndon, VA.